THE RATES OF ^{6}He(α,n)^{9}Be AND ^{4}He(2n,γ)^{6}He REACTIONS AND THE ASTROPHYSICAL r-PROCESS

Amy Jane Bartlett

A dissertation submitted to the Physics Department at the University of Surrey in partial fulfilment of the degree of Master in Physics.

Department of Physics

University of Surrey

April 25, 2004

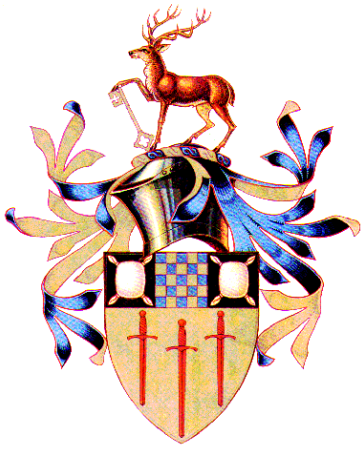

ABSTRACT

It has been thought that a possible site for the astrophysical r-process could be the shock fronts of supernovae explosions. In which case, the lack of stable nuclei with mass numbers of A=5 and 8, hinder the re-assemblage of seed nuclei from the free α-particles and nucleons. Consequently, the two reactions ^{6}He(α,n)^{9}Be and ^{4}He(2n,γ)^{6}He, could be of importance to any simulation of the r-process. Therefore, the rate of the ^{6}He(α,n)^{9}Be reaction was calculated by considering the resonances of ^{10}Be. An updated energy level description was used to calculate the reaction rate as a function of temperature. For temperatures $1.0 < T_9 < 5.0$ this gave values of the order $10^{-3} - 10^{1}$ cm^3 s^{-1} mol^{-1}. There are two mechanisms by which the ^{4}He(2n,γ)^{6}He reaction can occur. The first is by the successive capture of the two neutrons. The second is by dineutron capture. A numerical study was carried out of these rates. Previously only the successive capture rate had been estimated. Using an improved numerical quadrature, and a more recent value for $B(E2, 2^+ \rightarrow 0^+)$ in ^{6}He, the resonant rate was found to be 37% larger than previous estimates. However the direct capture rate matched the previous estimate. The dineutron capture rate is estimated here for the first time. It was found that the dineutron rate exceeded the successive capture rate by 2 to 3 orders of magnitude. Once these reaction rates had been calculated, the reactions ^{6}He(α,n)^{9}Be and ^{4}He(2n,γ)^{6}He could be included in r-process simulations. Three simulations of the r-process were run. The first did not include either reaction, the second and third both included the ^{4}He(2n,γ)^{6}He and ^{6}He(α,n)^{9}Be reactions, however in one the ^{4}He(2n,γ)^{6}He rate was set to the previous lower estimate of the reaction rate. The simulation with the previous ^{4}He(2n,γ)^{6}He rate and the simulation with no ^{4}He(2n,γ)^{6}He rate produced identical final element abundance curves, thus confirming that the previous ^{4}He(2n,γ)^{6}He rate estimate did not provide a significant flow towards heavier elements. The simulation with the new, increased, ^{4}He(2n,γ)^{6}He rate calculated here, did show an increased flow towards heavier nuclei, with

50% of the nuclei produced having A $\geq$ 95, as opposed to the other simulations which had 50% of nuclei with A $\geq$ 83. However, the inclusion of the 2 reactions, ^{4}He(2n,γ)^{6}He and ^{6}He(α,n)^{9}Be, causes a reduction in neutron abundance, which means the simulation terminates at a lower mass. The simulations did not run up to elements such as Bi and U. Further simulations should be run to investigate whether shorter timescales, and increased entropy, increase the mass number at which the simulations terminate. Also, none of the simulations run in this work duplicate any of the characteristic r-process peaks, since the simulations terminate before A=195; in actuality, they terminate at A$\sim$130. The only peak that might have been reproduced is the A=80 peak, but no pronounced peak is visible.

'There's coffee in that nebula!'

- Captain Kathryn Janeway

ACKNOWLEDGEMENTS

I would like to take this opportunity to thank Prof. Wiescher for allowing me the opportunity to study at the University of Notre Dame, South Bend Indiana, United States of America. And, to thank both Prof. Görres and Prof. Weischer for all their help with this work.

I would also like to thank Prof. Regan and Prof. Tostevin from the University of Surrey for their help and advice.

Also, thank you to all my friends, whose e-mails, letters, parcels and phone calls, made the distance between England and America feel that little bit smaller. Especially Sarah, who spent a small fortune on phone calls, and a larger fortune on air fares, and is now an expert at sending sandwich spread through the post.

Most importantly, I would like to thank my family; my Mum for putting up with many teary phone calls throughout my research year and whenever I've had exams; my Dad for all his support, both financial and otherwise; my sister for visiting me in America, so I wasn't alone for my 21st birthday; and my brother for sorting out my myriad computer problems and, more importantly, for making me laugh.

Contents

1 INTRODUCTION

Fusion processes in stars account for the nucleosynthesis of elements up to iron[1]. However, the abundances of heavy elements cannot be explained by charged-particle-induced fusion reactions, as these are inhibited by the increasing charge of heavier nuclei. Therefore, the heavy elements must be produced by some other process. That process is neutron capture.

There are two types of neutron capture, the s-process and the r-process. The s-process, or slow-neutron-capture process, is so called because the time between successive neutron captures exceeds the β-decay half lives of the unstable nuclei involved. Therefore this process takes place in nuclei in, or adjacent to, the valley of stability of the Segré chart. (See Figure (1).)

When neutrons are being captured much faster than the nuclei can β-decay, the process is classified as the r-process, or rapid-neutron-capture process. An r-process nucleus captures neutrons until the neutron binding energy approaches zero, this is called the neutron drip line, as shown in Figure (1). A nucleus on the drip line must then β-decay before neutron capture can continue. Therefore, unlike the s-process, the r-process proceeds along or near the drip line, far from the valley of stability. Unusually stable nuclei which contain a magic number of neutrons, or protons, are called waiting-point nuclei. These nuclei stall the flow towards heavier nuclei, with their long β-decay half lives. Both the s-process and r-process can be held up by waiting point nuclei.

A good approximation of r-process yields can be obtained by the subtraction of s-process yields from the observed solar elemental abundances. This r-process abundance curve exhibits distinct maxima at A=80, A=130 and A=195[1]. Therefore any r-process simulation needs to successfully reproduce these peaks and the relative abundances. The s-process exhibits peaks several mass units above these r-process peaks. This is due to the r-process reaching neutron magic numbers in lower Z nuclei. It is this fact, and that there are some naturally occurring radioactive elements, such as U and Th, which are above where the

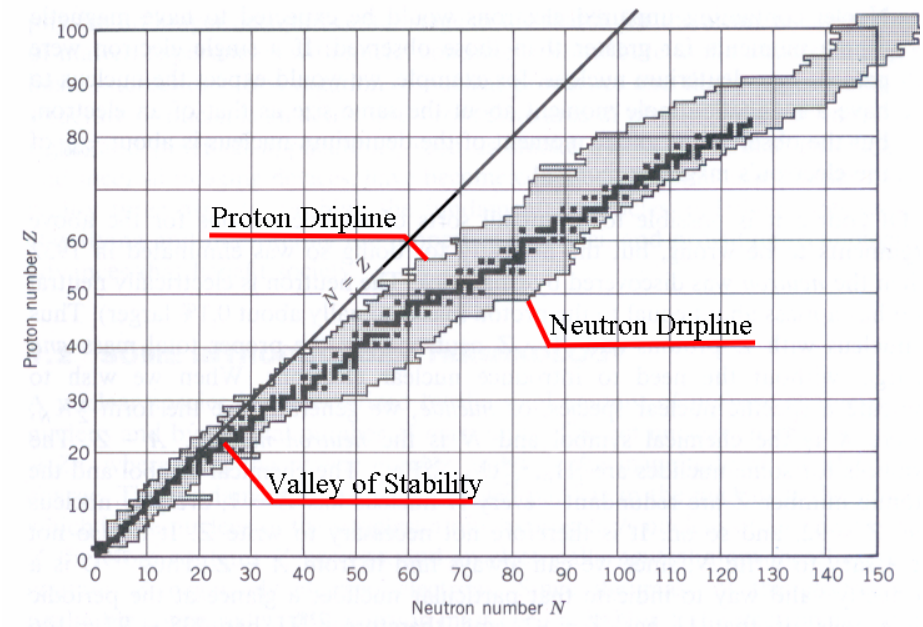

Figure 1: A Ségre chart from [5], modified to show the valley of stability as well as the neutron and proton drip lines.

s-process terminates, that lead physicists to the conclusion that there are two separate nucleosynthetic processes producing the heavy elements. Of the nuclei with A $\geq$ 70, there are 27 that can only be produced by the r-process[1].

The astrophysical site of the r-process is still an unanswered question. One favoured possible location is in the shockfronts of supernovae, as proposed by Woosley et al[2]. In this model the r-process occurs in the post-collapse phase of a type II supernova explosion, in which a neutron star is formed. After the neutron star formation and the shock heating of outer core material, neutrino heating occurs in the wake of the shock-front. This causes a high entropy hot bubble to form, which has a high proton to baryon ratio. The neutrino heating of this baryonic material causes movement. This neutrino induced mass outflow is called a neutrino-driven wind, and it is this that is believed to be a possible astrophysical site for the r-process. This baryonic matter is in Nuclear Statistical Equilibrium (NSE) and is initially composed of free α-particles and nucleons. The abundance distribution remains in NSE, but the neutrino

wind shifts it towards higher masses by the recombination of α's, protons and neutrons. However, there are no stable nuclei with mass numbers of 5 and 8. (See Table (1).) This causes a bottle-neck in the flow towards heavy nuclei because the reaction is controlled by the 3-particle fusion processes of 3 α's and 2α + n, which bridge these two mass numbers. It has been suggested that a series of two-neutron capture processes on ^{4}He and ^{6}He[3][6] could overcome this problem, since both ^{6}He and ^{8}He have unusually long halflives as they are halo nuclides. However, recent r-process simulations showed that the current, suggested reaction rates, were insufficient to provide a substantial flow towards heavy nuclei[7].

These mass numbers could also be bridged by the combination of the ^{4}He(2n,γ)^{6}He and ^{6}He(α,n)^{9}Be capture reactions. The ^{6}He(α,n)^{9}Be reaction is preferable to the ^{6}He(2n,γ)^{8}He reaction as the stable nucleus ^{9}Be is produced, which then links up to the ^{9}Be(α,n)^{12}C reaction to provide a flow towards heavier nuclei. Therefore rates need to be known for the ^{4}He(2n,γ)^{6}He and ^{6}He(α,n)^{9}Be reactions.

nuclide	$t_{1/2}$ / s [4]
^{3}He	stable
^{4}He	stable
^{5}He	7.6×10^{-22}
^{6}He	0.807
^{7}He	2.9×10^{-21}
^{8}He	0.119
^{9}He	1.5×10^{-21}
^{10}He	2.7×10^{-21}
^{5}He	7.6×10^{-22}
^{5}Li	3.0×10^{-22}
^{8}He	0.119
^{8}Li	0.838
^{8}Be	6.7×10^{-17}
^{8}B	0.770
^{8}C	2.0×10^{-21}

Table 1: Halflives of Helium isotopes and isobars of mass number 5 and 8.

2 THE REACTION RATE OF ^{6}He(α,n)^{9}Be

The reaction ^{6}He(α,n)^{9}Be is a compound nucleus reaction,

$$^6\mathrm{He} + \alpha \rightarrow {}^{10}\mathrm{Be}^{\star} \rightarrow^{9} \mathrm{Be} + n, \tag{1}$$

where ^{10}Be* is an excited state of the compound nucleus ^{10}Be. Such reactions occur when the incident particle, in this case the α-particle, has a small impact parameter compared with the radius of the target nucleus, in this case ^{6}He. (^{6}He has an extended nuclear radius since it is a halo nuclide.) This means that the α-particle is more likely to interact with one nucleon, rather than the entire target nucleus. The recoiling α-particle and nucleon go on to have successive interactions with other nucleons in the target, meaning that the energy of the incident α is shared among all the nucleons. The average increase in energy per nucleon is not enough to 'evaporate' them from the nucleus. However, there is a statistical distribution of energies, so there is a small probability that one or more nucleons will gain a sufficient fraction of the energy to escape the nucleus. The intermediate nucleus, after the α absorbtion and before neutron emission, is a compound nucleus. The decay of a compound nuclear state is almost entirely independent of its mode of formation.

2.1 THE ENERGY LEVELS OF ^{10}Be

The ^{6}He(α,n)^{9}Be reaction proceeds through excited states in ^{10}Be, therefore it is important to know the energy level structure of this nucleus. The threshold for this reaction is at 7.41 MeV, so only those energy levels above this threshold are considered here. The level scheme of Ajzenberg-Selove (1988)[8] has become outdated due to the many experiments performed since that data was evaluated. Figure (2) shows the revised energy level diagram used in the present reaction rate calculation.

There is a long-established state at 7.542 MeV, which is the first level that has the ^{6}He+α channel open to it. There is also a long-established state at

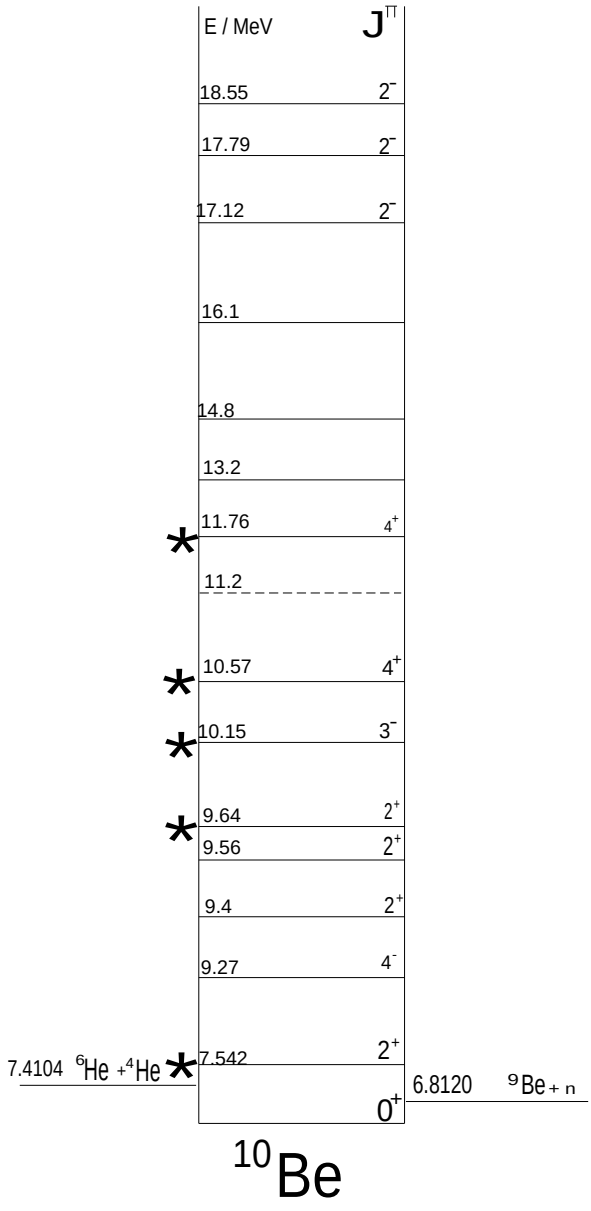

Figure 2: An energy level diagram for ^{10}Be, showing the energy levels above the ^{6}He + α threshold. The dashed line indicates that there is no conclusive evidence for that level's existence.

9.27 MeV, but this state has $J^\pi = 4^-$ so the ^{6}He + α channel is not open due to parity conservation. There is some debate about whether the next state quoted by [8] at 9.4 MeV exists, or whether it is the state later found at 9.64 MeV[9][10]. Since there is no conclusive evidence that a state at 9.4 MeV exists, it was not included in this reaction rate calculation. There is experimental evidence for states at 9.56[9][10] and 9.64 MeV[11][13]. These levels are close together and one is within the quoted experimental error on the other. In order not to overestimate the reaction rate, it was decided that only one of these levels would be included in the calculation. The 9.64 MeV $J^\pi = 2^+$ state was included. The next energy level at 10.15 MeV does not appear in [8]. It was originally quoted as 10.2 MeV $J^\pi = 4^+$[9] but was later found to be at 10.15 MeV with $J^\pi = 3^-$[11][13]. The level at 10.57 MeV is long established, however its spin and parity are in question. $J^\pi = 4^+$ was assumed for this calculation since a ^{12}C-like prolate model for ^{10}Be calls for a 4^+ state in this region[11] and the study of the ^{7}Li(α,p)^{10}Be (^{3}H transfer) reaction found evidence for a possible 4^+ state at either 10.15 or 10.57 MeV[12][14]. Since the 10.15 MeV state has been found to have $J^\pi = 3^-$[11] then the 10.57 MeV state is assumed to be the 4^+ state.

The next energy level at 11.76 MeV has yet to be assigned values for spin or parity, but values postulated so far include 4^+[10] and 5^-[12]. These are both high spin values, and bearing in mind this level is at high energy, its contribution to the cross-section at low energy is expected to be negligible. However, an assignment of $J^\pi = 4^+$ to this state would make interference possible with the 10.57 MeV state. Therefore, it was included in the calculation as a $J^\pi = 4^+$ state so that the role of this interference could be investigated.

In [12], the study of the reaction ^{12}C(^{12}Be,α^6He)^{14}C, found evidence of three new resonances in ^{10}Be at 13.2, 14.8 and 16.1 MeV. The resonance widths were measured to be $\sim$1 MeV each, and other resonances in this energy region have widths $\leq$ 500 keV, indicating that the natural widths of these states are being dominated by either the experimental resolution, or by contributions from several states. One of these resonances could be the 6^+ member of the 0+

rotational band, since this is predicted to be at 15.3 MeV[12]. However, since definite widths have not yet been determined for theses states and the proposed spins for these states are high, and would therefore present a high angular momentum barrier, indicating the cross-section contribution from these states at low energy would most likely be negligable, they were not included in the ^{6}He(α,n)^{9}Be rate calculation.

There are also three possible energy levels at 17.12, 17.79[8][10][11][13] and 18.55 MeV[8][10], all with $J^\pi = 2^-$. For the 17.12 and 17.79 MeV states the spin and parity was assigned from a comparison with ^{10}B, as in [10]. Out of these three levels the 17.79 MeV state has the most evidence pointing towards its existence, however these levels are not open to the ^{6}He+α entrance channel due to parity conservation.

Those levels included in the calculation are indicated by a * in Figure (2).

2.2 SPECTROSCOPIC FACTORS FOR THE ^{6}He(α,n)^{9}Be REACTION RATE CALCULATION

Table (2) contains the data necessary to calculate the ^{6}He(α,n)^{9}Be reaction rate.

The spectroscopic factors for the 9.64 and 10.57 MeV levels were approximated from the relative height of the peaks in Figure (3) in [9] . The 7.452 and 10.15 MeV spectroscopic factors had to be estimated.

The 10.15 MeV state does not decay into the ^{9}Be+n channel[9][12], so a C^2S_α was chosen so that the majority of the total width was equal to Γ_α. The 10.57 MeV state generally does not decay into the ^{6}He+α channel[12]. This state appears to be a member of a rotational band consisting of the 6.2 MeV $J^\pi = 0^+$, 7.542 MeV $J^\pi = 2^+$ and 10.57 MeV $J^\pi = 4^+$. Since the 10.57 MeV state does not decay into the α channel then it is reasonable to assume that the other members of the band also do not. Therefore spectroscopic factors were estimated for the 7.542 MeV state to reflect this.

E_R/MeV	J^π	Γ_{TOT}	$\Gamma_\alpha(E_R)$ (C^2S_α)	$\Gamma_n(E_R)$ (C^2S_n)	$\sigma(E_R)$
7.542	2^+	6.3×10^{-3}	8.64×10^{-8} (0.1)	6.299×10^{-3} (3.05×10^{-3})	$16.58\mu b$
9.64	2^+	0.291	0.034 (2.23×10^{-2})	0.26 (3.21×10^{-2})	96.8 mb
10.15	3^-	0.310	0.281 (0.40)	0.028 (8.51×10^{-3})	0.104 b
10.57	4^+	0.150	0.01 (5.03×10^{-2})	0.14 (0.23)	96.7 mb
11.76	4^+	0.121	0.104 (0.15)	0.017 (1.3×10^{-2})	0.170 b

Table 2: Data on resonances in ^{10}Be used to calculate the ^{6}He(α,n)^{9}Be reaction rate. The total width, Γ_{TOT}, and the partial widths, $\Gamma_\alpha(E_R)$ and $\Gamma_n(E_R)$, are all given in MeV. The spectroscopic factors corresponding to each partial width are given in brackets below the partial widths. The cross-section on resonance, $\sigma(E_R)$, is also given.

2.3 REACTION RATE THEORY

SPIN AND PARITY CONSERVATION

There are two factors affecting whether a resonant state can be formed by a given entrance channel; these are angular momentum conservation and parity conservation.

Angular momentum conservation can be described as

$$\boldsymbol{J_t} + \boldsymbol{J_p} + \boldsymbol{L} = \boldsymbol{J}, \tag{2}$$

where $\boldsymbol{J_t}$ and $\boldsymbol{J_p}$ are the spins of the target and projectile nuclei, $\boldsymbol{J}$ is the spin of the resonant state in the compound nucleus, and $\boldsymbol{L}$ is the relative angular momentum between the projectile and the target nuclei. A resonant state also cannot decay to a given exit channel, unless Equation (2) is obeyed. In the case of decay from a resonant state to an exit channel, $\boldsymbol{J_t}$ and $\boldsymbol{J_p}$ become the spins of the 2 particles in the exit channel.

Parity conservation is described as

$$\pi(\boldsymbol{J_t})\pi(\boldsymbol{J_p})(-1)^{\boldsymbol{L}} = \pi(\boldsymbol{J}). \tag{3}$$

In the reaction ^{6}He(α,n)^{9}Be, both the ^{6}He and the α-particle have ground state spin and parity of 0^+. This means that the ^{6}He+α entrance channel cannot form states in ^{10}Be with J^π=n^-_{even} or J^π=n^+_{odd}. (Where n_{even} is an even integer and n_{odd} is an odd integer.)

PARTIAL WIDTHS

Due to the Heisenberg uncertainty principle,

$$\Delta E \Delta t \geq \frac{\hbar}{2}, \tag{4}$$

a resonant state with a lifetime, τ, has associated with it, an energy width, Γ, by the relation

$$\Gamma = \frac{\hbar}{\tau}. \tag{5}$$

Γ can be determined experimentally by measuring the full-width-half-maximum (FWHM) of the resonant cross-section peak. A resonant state, with multiple exit channels, has associated with each exit channel a partial width, Γ_i. The total width of a given quantum state is given by the sum over the partial widths,

$$\Gamma_{TOT} = \sum_i \Gamma_i, \tag{6}$$

which in the case of the $^6He(\alpha, n)^9Be$ reaction is given by

$$\Gamma_{TOT} = \Gamma_\alpha + \Gamma_n. \tag{7}$$

Here the subscript α refers to the α-decay channel and the n indicates the neutron channel. The α and neutron widths can be calculated from the transmission values T_α and T_n,

$$\Gamma_\alpha = C^2 S_\alpha \, T_\alpha \quad \text{and} \quad \Gamma_n = C^2 S_n \, T_n. \tag{8}$$

The $C^2 S_{\alpha,n}$ are the respective spectroscopic factors. The transmission values were calculated in the RATE program (See Appendix I). Spectroscopic factors are a measure of the probability that the nucleus will be in the correct spatial configuration for the reaction to occur. Transmission values are a measure of the probability that the projectile will be able to tunnel through the angular momentum and Coulomb barriers of the target nucleus.

THE BREIT-WIGNER FORMULA

The energy dependent cross-section can be described by the Breit-Wigner formula, which applies to narrow isolated resonances. For a resonance at energy E_R, and with spin-parity J^π, the formula is[1]

$$\sigma(E) = \pi \bar{\lambda}^2 \omega \, \frac{\Gamma_\alpha \Gamma_n}{(E - E_R)^2 + (\Gamma_{TOT}/2)^2}, \tag{9}$$

where ω is the spin statistical factor. The spin statistical factor reflects the fact that an excited state of spin J, in a compound nucleus, has $2J + 1$ magnetic substates, and that the probability of the reaction occuring increases with the number of final states which can be formed. The entrance channel has $(2J_p + 1)(2J_t + 1)$ magnetic substate combinations, therefore the probability of the target and projectile nuclei being in a particular substate is inversely proportional to $(2J_p + 1)(2J_t + 1)$. Multiplying these two factors together gives ω, the spin statistical factor, which has been arrived at by summing over all the final states and averaging over the initial states. Therefore, for a final state J, ω is given by

$$\omega = \frac{2J + 1}{(2J_p + 1)(2J_t + 1)}. \tag{10}$$

The $\bar{\lambda}$ in Equation (9) is the de Broglie wavelength of the incident particle, given

by

$$\bar{\lambda} = \frac{m_p + m_t}{m_t} \frac{\hbar}{(2m_p E_l)^{\frac{1}{2}}}. \tag{11}$$

Here the subscripts p and t on the spins (J_p and J_t) and the masses (m_p and m_t) indicate the projectile and the target nuclei respectively. E_l is the laboratory energy of the projectile.

The term $\Gamma_\alpha \Gamma_n / [(E\text{-}E_R)^2 + (\Gamma_{TOT}/2)^2]$ in the Breit-Wigner formula (Equation (9)) is related to the probability, $P(E)$, of observing the the system in the energy range E to $E + dE$,

$$P(E)dE = \frac{dE}{(E - E_R)^2 + \left(\frac{\Gamma_{TOT}}{2}\right)^2}. \tag{12}$$

This relation comes from assuming a nuclear potential of the form $V + V'$, where V is the nuclear potential which gives stationary states[1] and V' is a small perturbing potential responsible for decay transitions. By solving the Schrödinger Equation for the potential V, the wave functions of the stationary states can be obtained. These wave functions can then be used to calculate the probability of transitions between stationary states, due to V'. The transition probability is given by Fermi's Golden Rule,

$$\Lambda = \frac{2\pi}{\hbar} |V'_{fi}|^2 \rho(E_f), \tag{13}$$

where

$$V'_{fi} = \int \Psi_f^\star V' \Psi_i dv. \tag{14}$$

Ψ_f and Ψ_i are the wave functions describing the final and initial states of the system. V'_{fi} is the matrix element of the perturbing interaction, V'. $\rho(E_f)$ is the density of final states, and is therefore the number of available final states per unit energy interval at E_f. The density of final states takes into account that

[1] A stationary state is a state with no width, Γ_{TOT}=0, since it doesn't decay. A stationary state is stable for all time, t, hence the term stationary.

the final state might not be isolated, this quantity is dependent upon the type of decay being discussed. The number of final states accessible to the system is $dn_f = \rho(E_f) dE_f$.

The Schrödinger Equation for the time independent potential, V, gives a stationary state wave function $\Psi_a(r)$, therefore the time-dependent wave function for the stationary state, a, is given by

$$\Psi_a(r,t) = \Psi_a(r) e^{-iE_a t/\hbar}, \tag{15}$$

where E_a is the energy of state a. Since the probability density of finding the system with position, r, at time, t, in a state, a, is $|\Psi_a(r,t)|^2$, which is independent of time for a stationary state. The radioactive decay law demands that the probability of decay decreases with increasing time as $\sim e^{-t/\tau_a}$, where τ_a is the mean lifetime of the state. Therefore the time dependent probability is

$$|\Psi_a(t)|^2 = |\Psi_a(t=0)| e^{-t/\tau_a} \tag{16}$$

and the wave function $\Psi_a(r,t)$ is given by

$$\Psi_a(\boldsymbol{r},t) = \Psi_a(\boldsymbol{r}) e^{-iE_a t/\hbar} e^{-t/(2\tau_a)}. \tag{17}$$

The distribution of energy states is given by the Fourier transform of $e^{-t/(2\tau_a)}$, and the probability of observing the system in the energy interval E to $E + dE$ is given by the square of this distribution, thus giving Equation (12).

CALCULATING THE CROSS SECTION

The cross-section on resonance, σ_R, is given by

$$\sigma_R = \sigma(E_R) = 4\pi \bar{\lambda}_R^2 \, \frac{\omega\gamma}{\Gamma_{TOT}}, \tag{18}$$

where the resonance strength, γ, has been introduced, where

$$\gamma = \frac{\Gamma_\alpha \Gamma_n}{\Gamma_{TOT}}. \tag{19}$$

Therefore, it follows that the energy-dependent cross-section can be calculated for any energy, E, as

$$\sigma(E) = \sigma_R \left(\frac{E_R}{E}\right) \frac{\Gamma_\alpha(E)}{\Gamma_\alpha(E_R)} \frac{\Gamma_n(E)}{\Gamma_n(E_R)} \frac{(\Gamma_{TOT}(E_R)/2)^2}{(E-E_R)^2 + (\Gamma_{TOT}(E)/2)^2}. \tag{20}$$

Equation (20) only calculates the cross-section contribution from a single resonance. Since there are many levels in ^{10}Be, the cross-sections from each non-overlapping level must be summed to give the total cross-section

$$\sigma_{TOT}(E) = \sum_i \sigma_i(E). \tag{21}$$

INTERFERENCE IN THE CROSS SECTION

When summing the σ_i's, interference between pairs of states with the same J^π can be taken into account by the equation

$$\sigma_{int}(E) = \sigma_1(E) + \sigma_2(E) \pm 2\sqrt{\sigma_1(E)\sigma_2(E)}\delta, \tag{22}$$

where

$$\delta = \arctan\left(\frac{\Gamma_{TOT_{R1}}(E)/2}{E_{R1}-E}\right) - \arctan\left(\frac{\Gamma_{TOT_{R2}}(E)/2}{E_{R2}-E}\right). \tag{23}$$

Here the subscripts 1 and 2 indicate the two energy levels between which the interference can occur.

There are two pairs of energy levels for which interference may be relevant in ^{10}Be*. These are the 9.64 MeV and 7.542 MeV, $J^\pi = 2^+$ states and the 10.57 MeV and 11.76 MeV, $J^\pi = 4^+$ states. Although the interference between the $J^\pi = 4^+$ states was significant, it was, nevertheless, negligible at the low energies from which the reaction rate was calculated. The interference between the

$J^\pi = 2^+$ states was also found to be negligible since the states are well separated in energy. Therefore, these interference effects have no practical significance in the present example.

CALCULATING THE REACTION RATE

The reaction rate is given by

$$r = N_t N_p \, v \, \sigma(v). \tag{24}$$

Since the cross-section is a function of energy, it is also a function of velocity, $\sigma(v)$, where v is the relative velocity between the target and projectile nuclei. It is assumed that the target is initially stationary. N_t and N_p are the number density of the target and projectile nuclei respectively. Equation (24) is the product of the effective area of target nuclei per cm^3, given by $N_t\sigma(v)$, and the flux of the incident projectile nuclei per cm^3, given by $N_p v$. The rate, r, is usually given in units of cm^{-3} s^{-1}.

The reactions discussed here occur in a gaseous environment, in which the particles have a distribution of velocities, $\phi(v)$, where

$$\int_0^\infty \phi(v) dv = 1. \tag{25}$$

$\phi(v)\ dv$ is the probability that the relative velocity between the target and projectile will be in the range v to $v + dv$. Therefore the product $v\sigma(v)$ in Equation (24) has to be folded with the velocity distribution to give a value of $v\sigma(v)$ averaged over the velocity distribution,

$$<\sigma v> = \int_0^\infty \phi(v) v\sigma(v) dv. \tag{26}$$

The total rate, r, is now given by

$$r = N_t N_p <\sigma v> . \tag{27}$$

The quantity $<\sigma v>$ is the reaction rate per particle pair and is given in units of cm^3 s^{-1}. It is $<\sigma v>$ that must be calculated to implement a reaction in r-process simulations.

Despite the high temperatures involved in the r-process (up to 10^{10}K = 10GK = 10T$_9$), the material in the neutrino-driven-wind is non-degenerate and moves non-relativistically. This means that the velocity distributions, of both the target and projectile nuclei, are given by a Maxwell-Boltzmann velocity distribution,

$$\phi(v_t) = 4\pi v_t^2 \left(\frac{m_t}{2\pi kT}\right)^{\frac{3}{2}} \exp\left(\frac{-m_t v_t^2}{2kT}\right), \tag{28}$$

and

$$\phi(v_p) = 4\pi v_p^2 \left(\frac{m_p}{2\pi kT}\right)^{\frac{3}{2}} \exp\left(\frac{-m_p v_p^2}{2kT}\right). \tag{29}$$

The velocities, v_t and v_p, can be converted to the centre-of-mass reference-frame velocities, v and V respectively, giving

$$\phi(v) = 4\pi v^2 \left(\frac{\mu}{2\pi kT}\right)^{\frac{3}{2}} \exp\left(\frac{-\mu v^2}{2kT}\right), \tag{30}$$

and

$$\phi(V) = 4\pi V^2 \left(\frac{M}{2\pi kT}\right)^{\frac{3}{2}} \exp\left(\frac{-M V^2}{2kT}\right), \tag{31}$$

which has made use of the reduced mass, $\mu = (m_p m_t)/(m_p + m_t)$, and the total mass, $M = m_p + m_t$, has been introduced. Substituting into Equation (26) gives

$$<\sigma v> = \int_0^\infty \int_0^\infty \phi(V)\phi(v)\sigma(v) v dV dv, \tag{32}$$

$$= \int_0^\infty \phi(v)\sigma(v) v dv \int_0^\infty \phi(V) dV, \tag{33}$$

$$= \int_0^\infty \phi(v)\sigma(v)v dv, \tag{34}$$

since both Maxwell-Boltzmann velocity distributions are normalised to 1, as in Equation (25). Substituting Equation (30) into Equation (34) gives

$$<\sigma v>= 4\pi \left(\frac{\mu}{2\pi kT}\right)^{\frac{3}{2}} \int_0^\infty v^3 \sigma(v) \exp\left(\frac{-\mu v^2}{2kT}\right) dv. \tag{35}$$

Then, substituting in for v, using $E = \frac{1}{2}\ \mu\ v^2$, for the centre-of-mass energy, gives

$$<\sigma v>= \left(\frac{8}{\pi\mu}\right)^{\frac{1}{2}} \frac{1}{(kT)^{\frac{3}{2}}} \int_0^\infty \sigma(E) E \exp\left(\frac{-E}{2kT}\right) dE. \tag{36}$$

2.4 RESULTS AND DISCUSSIONS

Figure (4) shows the dependence of the total cross-section on the centre-of-mass energy, for the ^{6}He(α,n)^{9}Be reaction. Both axes are logarithmic and the cross-section decreases rapidly as the energy approaches zero. The lowest energy peak is the 7.542 MeV energy level. The other peaks, at higher energy, are the 9.64, 10.15 and 10.57 MeV levels in ^{10}Be. Figure (4) also shows the individual cross-section contributions from each resonance. This shows that the 7.542 MeV energy level dominates the cross-section at low incident energies (E $<$ 0.3 MeV) whilst the other peaks dominate at higher energies.

Figure (4) presents the calculated reaction rates as a function of temperature for the ^{6}He(α,n)^{9}Be reaction. The reaction rate curve is not smooth because of the resonances in the cross-section. A Functional fit was found so that the reaction rate could be included in r-process simulations. (See Appendix III for further details.)

2.5 CONCLUSION

The temperature dependence of the ^{6}He(α,n)^{9}Be reaction rate was determined. A FORTRAN program was written to calculate the total cross-section by sum-

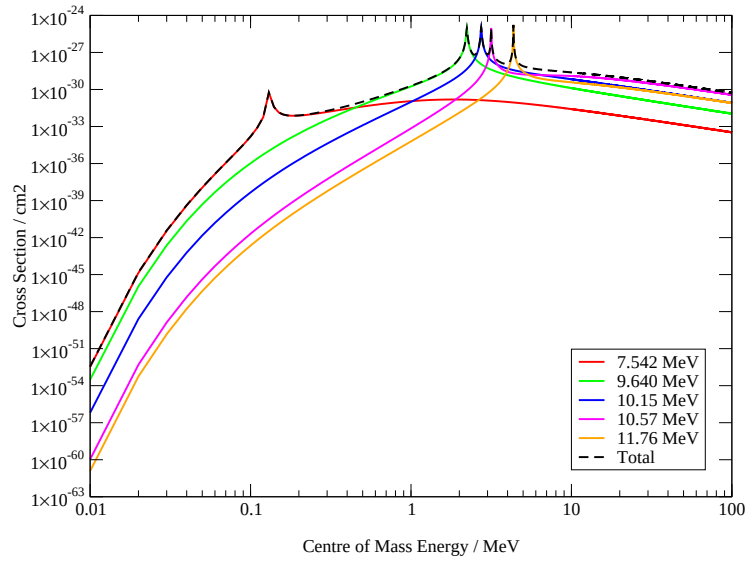

Figure 3: Total cross-section in cm^2 against energy in MeV for the reaction ^{6}He(α,n)^{9}Be.

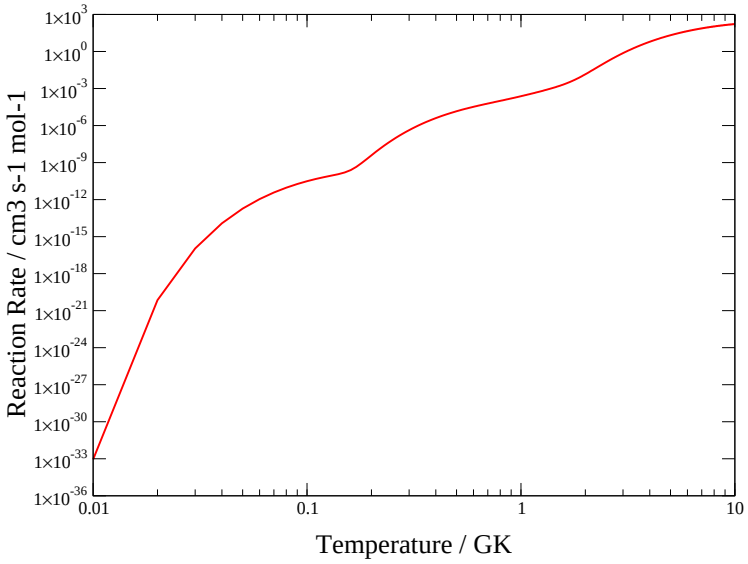

Figure 4: Reaction rate in cm^3 s^{-1} mol^{-1} against temperature in GK for the reaction $^6He(\alpha,n)^9Be$, and a fit to this data.

T_9	$N_A <\sigma v>_{TOT}$
0.5	1.44×10^{-5}
0.8	9.99×10^{-5}
1.0	2.38×10^{-4}
1.5	1.55×10^{-3}
2.0	2.81×10^{-2}
2.5	2.37×10^{1}
3.0	1.03×10^{0}
4.0	6.32×10^{0}
5.0	1.82×10^{1}

Table 3: This table shows the calculated total reaction rate in cm^3 s^{-1} mol^{-1} for different temperatures in GK, for the reaction ^{6}He(α,n)^{9}Be.

ming the cross-section contributions from the different energy levels in ^{10}Be. The Breit-Wigner formula was used to calculate the cross-sections from the individual resonances. Temperatures in the region of $1.0 \leq T_9 \leq 5.0$ yield reaction rates of the order of 10^{-3} to 10^{1} cm^3 S^{-1} mol^{-1}.

3 THE REACTION RATE OF ^{4}He(2n,γ)^{6}He

Two mechanisms are discussed here, by which the reaction ^{4}He(2n,γ)^{6}He can take place. These are successive neutron capture (SNC) and simultaneous neutron (dineutron) capture (DNC). For the purposes of this work the symbol ^2n is used to represent the dineutron in nuclear reactions. It is assumed that dineutron is a neutral particle that behaves like a neutron except it has double the mass.

SUCCESSIVE CAPTURE OF 2 NEUTRONS

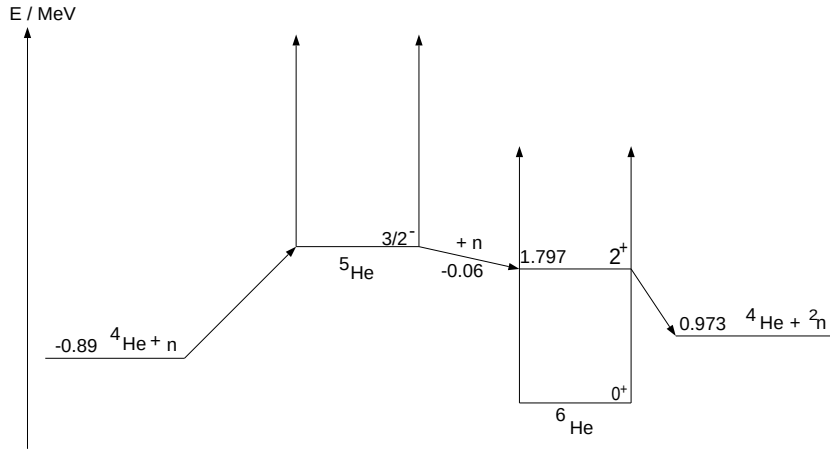

Figure 5: Diagram showing the successive capture of 2 neutrons on ^{4}He.

In [3], Goerres et al. estimated the reaction rate for the successive capture of two neutrons on ^{4}He. The intermediate nucleus, ^{5}He, is unbound, the lowest state being a $\frac{3}{2}^-$ resonance. However, there can nevertheless be an equilibrium abundance of ^{5}He, on which the second neutron can be captured to form ^{6}He. This forms an excited 2^+ state in ^{6}He, 1.8 MeV above the ground state. This $J^\pi = 2^+$ state is below the 1 neutron threshold, but is open to decay by 2n emission, therefore the ^{5}He(n,γ)^{6}He reaction can proceed through the low energy

tail of this broad resonance. This reaction is described by the equations below,

$$^4\mathrm{He} + \mathrm{n} + \mathrm{n} \rightarrow {}^5\mathrm{He} + \mathrm{n} \rightarrow {}^6\mathrm{He}^\star \rightarrow {}^6\mathrm{He} + \gamma, \quad (37)$$

$$\rightarrow {}^4\mathrm{He} + {}^2n. \quad (38)$$

DINEUTRON CAPTURE

DNC differs from SNC since both the neutrons are captured on the ^{4}He simultaneously. The two neutrons are assumed to have formed a localised dineutron. Like ^{5}He, the dineutron is unbound. However the experimentally determined n-n scattering cross-section exhibits a 'virtual' state near zero energy, indicating that the dineutron state is close to being bound. Once the dineutron is captured on the ^{4}He, the 1.8 MeV resonance in ^{6}He is formed and the reaction then proceeds in the same way as for the successive capture route, as shown in the following equation

$$^4\mathrm{He} + \mathrm{n} + \mathrm{n} \rightarrow {}^4\mathrm{He} + {}^2\mathrm{n} \rightarrow {}^6\mathrm{He}^\star \rightarrow {}^6\mathrm{He} + \gamma. \quad (39)$$

THE GAMMA DECAY OF ^{6}He

The 1.8 MeV $J^\pi=2^+$ state can γ-decay into the 0^+ ground state. γ-decay is caused by oscillating charge or current distributions in the nucleus, which are associated with electric or magnetic multipole moments[5]. The type of transition observed depends on angular momentum and parity conservation. A photon must carry away at least 1 unit of angular momentum. The multipole order of the radiation, L, is numerically equal to the angular momentum of the photon. Since no one has ever observed a magnetic monopole, and the electric monopole is simply the electric charge of the nucleus, which does not vary with time, the lowest multipoles possible are the magnetic and electric dipoles. Thus meaning the photon must carry away a minimum of 1 unit of angular momentum. The parity of a transition is given by

$$\pi_M(L) = (-1)^{L+1} \quad \text{and} \quad \pi_E(L) = (-1)^L. \tag{40}$$

Where π_M and π_E are the parities of magnetic and electric transitions, respectively.

Therefore, in the case of ^{6}He, $J^\pi = 2^+ \rightarrow 0^+$ transition, only electric quadrupole radiation is observed. However, in the case of a ^{2}n being directly captured into the ground state of ^{6}He, other multipole radiations are possible, since this mechanism does not go through the 2^+ resonance. In fact when calculating the direct capture cross-section for dineutron capture on ^{4}He, it was found that E1 (electric dipole) transitions provided the largest cross section, and was therefore the dominant γ-decay mechanism.

In [3] a value of B(E2,$2^+ \rightarrow 0^+$)=0.57 e^{2}fm^4 for the electric quadrupole transition strength was used to calculate the γ-decay width, Γ_γ,

$$\Gamma_\gamma = \frac{2(L+1)}{\epsilon_0 L[(2L+1)!!]^2} \left(\frac{E_\gamma}{\hbar c}\right)^{2L+1} B(E2, 2^+ \rightarrow 0^+). \tag{41}$$

Here E_γ is the energy of the emitted γ-decay photon, which in the case of resonant capture, is equal to 1.8 MeV. In [15] a value of B(E2,$0^+ \rightarrow 2^+$)= (3.2 $\pm$ 0.6) e^{2}fm^4 was determined experimentally from the three-body breakup of ^{6}He. The B(E2,$0^+ \rightarrow 2^+$) is related to the B(E2,$2^+ \rightarrow 0^+$) by the relation

$$\begin{aligned} B(E2, 2^+ \rightarrow 0^+) &= \frac{1}{(2L+1)} B(E2, 0^+ \rightarrow 2^+), & (42)\\ &= \frac{1}{5} \times B(E2, 0^+ \rightarrow 2^+), & (43)\\ &= 0.64 \text{ e}^2\text{fm}^4. & (44) \end{aligned}$$

Therefore a new γ-decay width of 9.88 μeV, calculated using Equation (41), was used in the following work.

DIRECT CAPTURE

The second step in the reaction ^{4}He(2n,γ)^{6}He, (either ^{5}He+n or ^{4}He+^{2}n) can proceed via direct capture. Direct reactions are also known as peripheral reactions since they occur at the surface of the target nucleus[5]. The cross-section for direct reactions, such as direct capture, increases with energy as the de Broglie wavelength of the projectile decreases with energy. A smaller de Broglie wavelength, comparable to the size of a nucleon, rather than the target nucleus as a whole, is more conducive to direct reactions.

The direct capture cross-section for the ^{4}He(^{2}n,γ)^{6}He reaction was initially calculated in a program called JEZEBEL (See Appendix I). JEZEBEL uses a hard sphere model of the nucleus and a diffuse Woods-Saxon potential to calculate the cross-section. A diffuseness of a=0.6 fm was used and the optimal well depth was found in the program. The formalism for JEZEBEL is described in [23], except that the square-well potential has been replaced with a Woods-Saxon. Modelling the nucleus as a hard sphere is adequate only for reactions with a high Coulomb and/or angular momentum barrier. The JEZEBEL program showed that electric dipole (E1) transitions were dominant, providing a cross-section 5 orders of magnitude larger than electric quadrupole (E2) transitions. Therefore only the E1 cross-section was considered. However, there is no Coulomb barrier for a dineutron and there is only an angular momentum change of 1 unit, therefore assuming the nucleus to be a hard sphere is not sufficient. Therefore, the direct capture cross-section was calculated by Mengoni, as in [25].

The cross-section was calculated from[25]

$$\sigma_{^2n,\gamma} = \frac{16\pi}{2\hbar} k_\gamma^3 \bar{e}^2 |Q_{i\to f}|^2, \tag{45}$$

where k_γ=$E_\gamma\hbar c$ and $\bar{e}$ is the effective charge for E1 neutrons/dineutrons, given by

$$\bar{e} = \frac{-eZ}{A}. \tag{46}$$

The cross-section is determined by the matrix elements

$$Q^{(1)}_{i\to f} =< \Psi_f|\hat{T}^{E1}|\Psi_i >, \tag{47}$$

where $\hat{T}^{E1}$ is the electric dipole operator and Ψ_i and Ψ_f are wave functions describing the initial and final states respectively. The Mengoni direct capture cross-section was smaller than that calculated in JEZEBEL, but it was of the same form. The Mengoni cross-section was not calculated over a sufficiently large range of energies to determine the reaction rate up to $10\mathrm{T}_9$. Therefore the JEZEBEL cross-section was scaled down to match the Mengoni cross-section. The Mengoni cross-section was on average 25% smaller than the JEZEBEL cross-section.

3.1 TWO-STEP CAPTURE THEORY

Both SNC and DNC are two-step reactions, consequently the reaction rate for both these reactions is described by a double integral,

$$N_A^2 <1pp>= N_A^2 \int_{E_1} \frac{d<(p,p)>(E_1)}{dE_1} \frac{2\hbar}{\Gamma(E_1)} \left[\int_{E_2} \frac{d<p,\gamma>(E_1,E_2)}{dE_2} dE_2\right] dE_1, \tag{48}$$

where the integrands are given by

$$\frac{d<\sigma v>}{dE} = \sqrt{\frac{8}{\pi\mu}} \frac{1}{(kT)^{\frac{3}{2}}} \sigma(E)\ \exp\left(-\frac{E}{kT}\right), \tag{49}$$

where p indicates particle. This is the same notation as that used in [3]. $<1pp>$ is the three-body reaction rate. In the case of successive capture $<(p,p)>$ refers to the rate of capture of the first neutron on ^{4}He and E_1 is the collision energy of this first neutron, while $<p,\gamma>$ refers to the rate of capture of the second

neutron on ^{5}He and E_2 is the collision energy of this neutron. $\Gamma_2(E_1)$ is the energy dependent width of the intermediate nucleus, which in this case is the width of the $\frac{3}{2}^-$ state in ^{5}He. In the case of dineutron capture the width of the intermediate state would be the width of the dineutron virtual state. In which case, $<(p,p)>$ now refers to the rate of formation of the dineutron, E_1 is the neutron collision energy, $<p,\gamma>$ refers to the dineutron capture rate on ^{4}He, and E_2 is the dineutron collision energy.

3.2 THE CALCULATION

In [3] a FORTRAN program called TWOSTEP was used to calculate the SNC rate. (More details on the program TWOSTEP are available in Appendix I.) This program was adapted so that it could be used to calculate the SNC rate more efficiently and then later adapted further to enable the calculation of the DNC rate.

The subroutines originally performing the integrations in Equation (48) in TWOSTEP used a fixed step-size and, for the program to perform to the required accuracy, the execution time was considerable. These integration subroutines were replaced by a subprogram from the CERN library, which uses adaptive Gaussian quadrature to calculate the value of an integral. This subprogram varies the step size across the interval, depending on how quickly the function being integrated is changing. This enabled the program to run much faster, and consequently the reaction rate could be calculated to higher accuracy and the limits of integration extended.

3.3 RESULTS AND DISCUSSIONS

SUCCESSIVE NEUTRON CAPTURE

The updated value for B(E2,$2^+ \rightarrow 0^+$), combined with the greater accuracy of the new integration subprogram, gave the results shown in Figure (6).

Figure (6) shows the original RC values published in [3], and the new values,

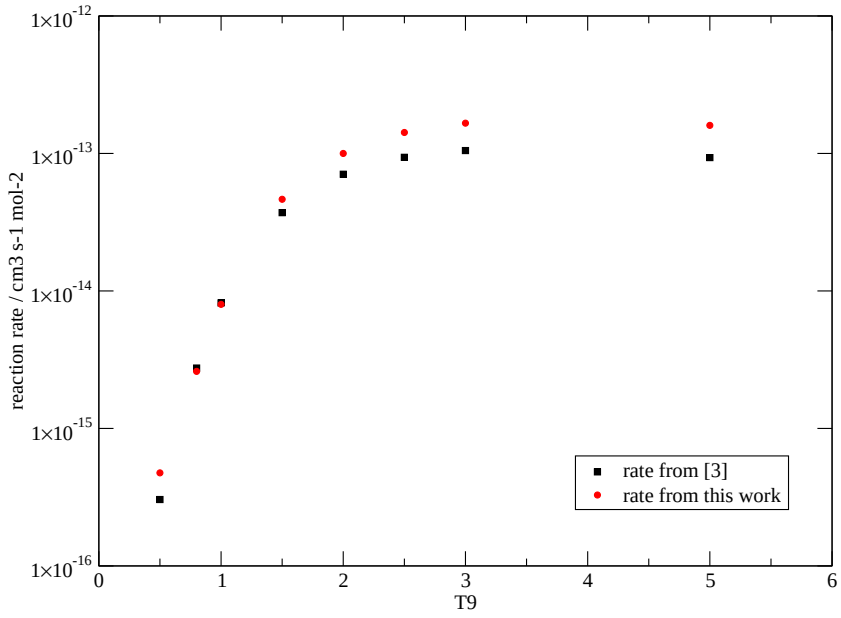

Figure 6: Reaction rate against temperature in GK for the successive capture of 2 neutrons on ^{4}He. The squares indicate the values published in [3], the circles indicate the new values.

which were calculated for the same temperatures. On average the new values are 37% larger than the previous estimates. Table (4) shows the RC values used to produce Figure (6), as well as the direct capture (DC) rate published in [3].

Although the new values are larger, they are the same order of magnitude as the original estimates. Since the original estimates were not sufficient to provide a substantial flow towards heavy nuclei in r-process simulations[7], it is evident that the new values would not significantly change that.

DINEUTRON CAPTURE

The dineutron reaction rate was calculated by adapting the TWOSTEP program (See Appendix I.) used to calculate the SNC rate. In the case of DNC the first step in the reaction is the formation of the dineutron from its constituent neutrons. The second step is the capture of the dineutron on ^{4}He. A fit to

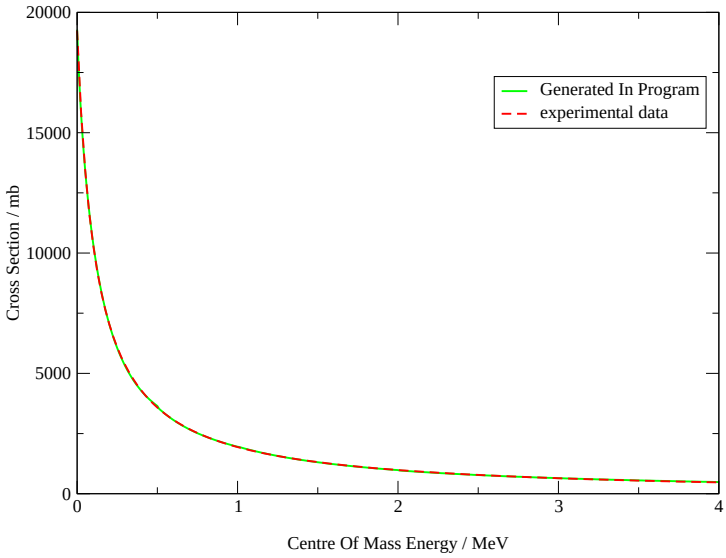

Figure 7: The Dineutron formation (or n-n scattering) cross-section against energy. The dotted curve is the experimentally determined cross-section, the solid curve is the dineutron cross-section produced as output from the TWOSTEP program.

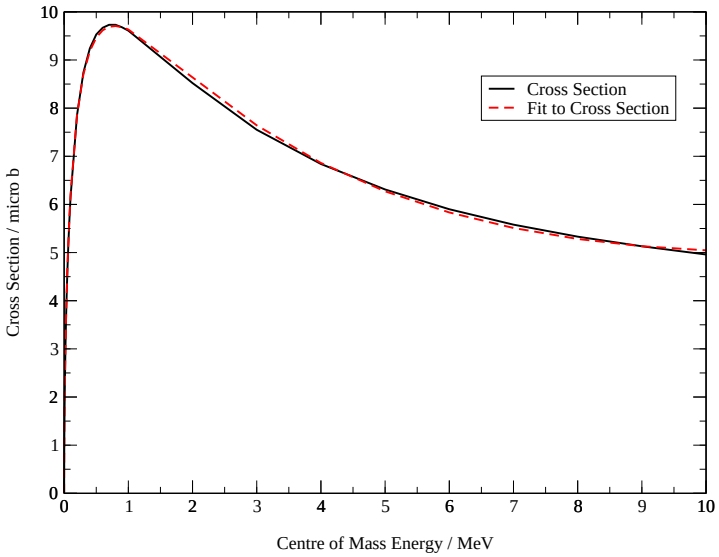

Figure 8: The Dineutron direct capture cross-section on ^{4}He (the solid curve) and a fit to that cross-section (the dotted curve).

T_9	$N_A^2 <{}^4He2n>$		
	DC	Resonant	
	[3]	[3]	This Work
0.5	4.00×10^{-11}	3.04×10^{-16}	4.75×10^{-16}
0.8	8.00×10^{-11}	2.75×10^{-15}	2.60×10^{-15}
1.0	1.15×10^{-10}	8.18×10^{-15}	7.99×10^{-15}
1.5	2.20×10^{-10}	3.71×10^{-14}	4.64×10^{-14}
2.0	3.29×10^{-10}	7.06×10^{-14}	1.00×10^{-13}
2.5	4.25×10^{-10}	9.37×10^{-14}	1.42×10^{-13}
3.0	5.01×10^{-10}	1.05×10^{-13}	1.66×10^{-13}
5.0	6.49×10^{-10}	9.33×10^{-14}	1.60×10^{-13}

Table 4: Reaction rates for the successive capture of two neutrons on ^{4}He, for different temperatures, T_9. Both the direct capture and resonant rates published in [3] are tabulated here, as well as numbers produced in this work.

experimental data was used to provide the dineutron formation cross-section. (See Appendix III for details.)

Figure (7) shows the experimental two-neutron cross-section[26], and the dineutron cross-section output from the program TWOSTEP, which uses fits to the experimental data to reproduce the cross-section curve. (See Appendix III for details.)

The dineutron state is not a resonance, but it has been treated as such in this calculation. It is in fact a 'virtual' state. The energy dependence of the width

T_9	$N_A^2 <{}^4He2n>$	
	DC	Resonant
0.5	2.44×10^{-8}	3.68×10^{-15}
0.8	4.06×10^{-8}	4.79×10^{-14}
1.0	5.06×10^{-8}	1.88×10^{-13}
1.5	7.19×10^{-8}	1.11×10^{-12}
2.0	8.88×10^{-8}	2.24×10^{-12}
2.5	1.02×10^{-7}	3.00×10^{-12}
3.0	1.13×10^{-7}	3.32×10^{-12}
5.0	1.39×10^{-7}	2.75×10^{-12}

Table 5: Reaction rates for both direct capture (DC) and resonant dineutron capture on ^{4}He for different temperatures.

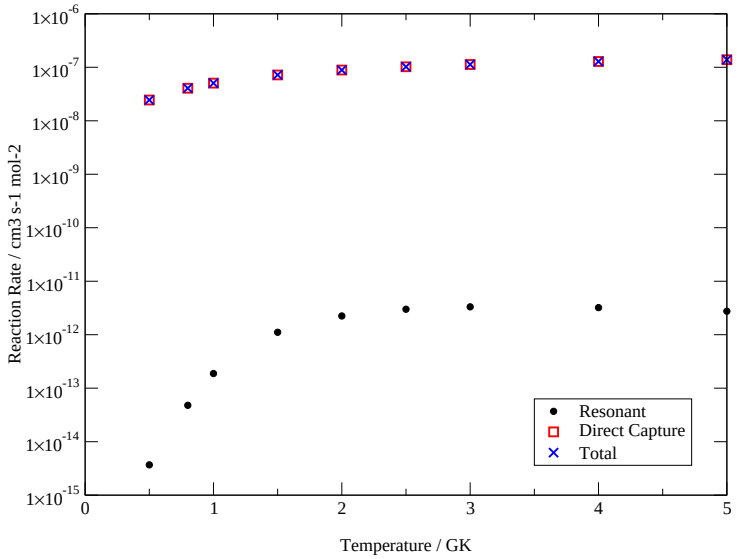

Figure 9: The Resonant and direct capture rates for dineutron capture on ^{4}He, agianst temperature in GK. The sum of these two rates is also plotted, and is labelled total.

of this virtual state is needed so that Equation (48) can be used to calculate the reaction rate. The dineutron width was set as a constant, equal to the FWHM of the experimental curve shown in Figure (7), which is 0.095 MeV.

There are two mechanisms by which the dineutron can be captured on ^{4}He, resonant capture (RC) and direct capture (DC). In RC the dineutron is captured to form the 1.797 MeV $J^\pi = 2^+$ resonance state, which can then γ-decay to the ground state. In direct capture the reaction bypasses the resonance state and is 'directly' captured into the ground state of ^{6}He.

Figure (9) shows the RC rate, the DC rate and the total reaction rate, which is given by the sum of the RC and DC rates. The total rate is entirely dominated by the DC rate. Table (5) shows the values used to produce Figure (9). It clearly shows that for $0.5 \leq T_9 \leq 5.0$, the RC rate is $\sim 5 \rightarrow 7$ orders of magnitude smaller than the DC rate.

COMPARISON BETWEEN SUCCESSIVE CAPTURE RATES AND DINEUTRON CAPTURE RATES

Table (6) shows the total rates for both the successive capture of two neutrons on ^{4}He and dineutron capture. Although the resonant, successive capture rate is 37% larger than previous values, it is negligible in comparison with the DC rate, which has in turn been shown to be negligible in comparison with the dineutron capture rate. The dineutron capture rate is 2 to 3 orders of magnitude larger than the successive rate.

3.4 CONCLUSION

The FORTRAN program used in [3] was updated and modified, so that it could be used to calculate the successive neutron capture rate and the dineutron capture rate on ^{4}He. Improved numerical integration and an updated $B(E2, 2^+ \rightarrow 0^+)$ yielded resonant successive neutron capture rates 37 % larger than previous estimates. However, this improvement is negligible in comparison with the dineutron capture rate which is 2 to 3 orders of magnitude larger.

T_9	$< \sigma v >_{TOT}$		
	^2n Capture	$n+n$ Capture	
		This Work	[3]
0.5	2.44×10^{-8}	4.00×10^{-11}	4.00×10^{-11}
0.8	4.06×10^{-8}	8.00×10^{-11}	8.00×10^{-11}
1.0	5.06×10^{-8}	1.15×10^{-10}	1.15×10^{-10}
1.5	7.19×10^{-8}	2.20×10^{-10}	2.20×10^{-10}
2.0	8.88×10^{-8}	3.29×10^{-10}	3.29×10^{-10}
2.5	1.02×10^{-7}	4.25×10^{-10}	4.25×10^{-10}
3.0	1.12×10^{-7}	5.01×10^{-10}	5.01×10^{-10}
4.0	1.28×10^{-7}	6.49×10^{-10}	6.49×10^{-10}
5.0	1.39×10^{-7}	6.49×10^{-10}	6.49×10^{-10}

Table 6: The total reaction rates for both dineutron and successive neutron capture, where the total rate is the sum of the direct capture and resonant reaction rates. The reaction rates are given in cm^3 mol^{-2} s^{-1}. The temperature is given in GK.

4 THE REACTION RATE OF ^{6}He(α,n)^{9}Be REVISITED

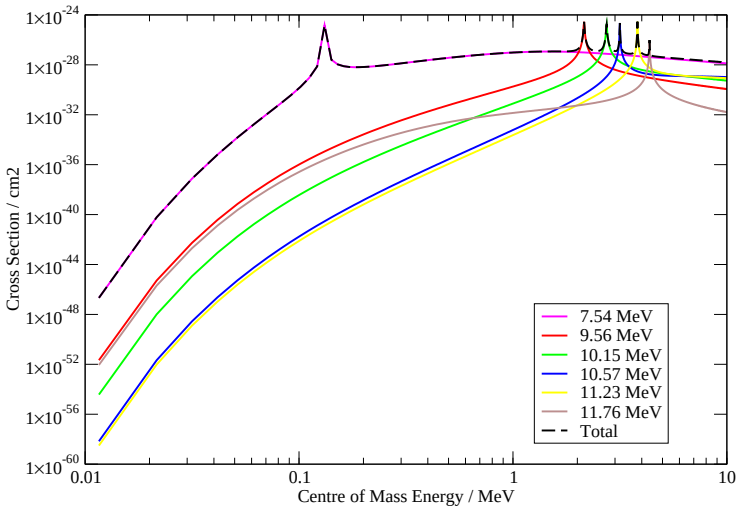

Figure 10: The cross-section against centre-of-mass energy for the ^{6}He(α,n)^{9}Be reaction. The cross-section was calculated from the revised ^{10}Be level scheme in [20].

A new evaluation of experimental data by TUNL resulted in a revised energy level scheme for ^{10}Be[20]. Using this revised level scheme, a new calculation of the cross-section and rate of the ^{6}He(α,n)^{9}Be reaction was performed.

Figure (10) shows the cross-section calculated from the revised level scheme. This cross-section is 5 orders of magnitude larger than the cross-section shown in Figure (3) for a centre-of-mass energy, E_{CM}, of 0.01 MeV. However between $1 \leq E_{CM} \leq 10$ MeV, there is little difference in the cross-section.

Figure (11) shows the reaction rate calculated for the revised energy level scheme. In comparison with the previous reaction rate shown in Figure (4), the rate is 3 orders of magnitude larger at $E_{CM} = 0.1$. There is still a similar order of magnitude difference at E_{CM}=1 MeV, however at 10 MeV, the rates are very

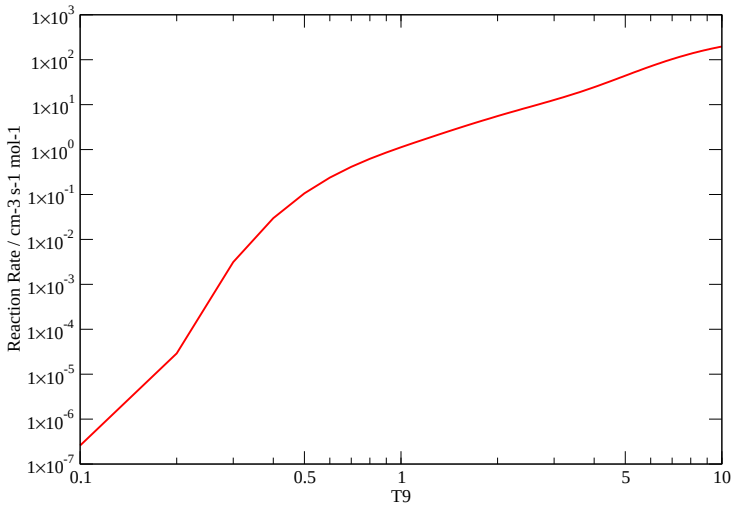

Figure 11: Reaction rate against temperature for the reaction ^{6}He(α,n)^{9}Be. The revised level scheme of ^{10}Be in [20] was used to calculate the reaction rate.

E_R/MeV	J^π	$\Gamma_{TOT}(E_R)$	$\Gamma_\alpha(E_R)$ (C^2S_α)	$\Gamma_n(E_R)$ (C^2S_α)	$\sigma(E_R)$
7.542	2^+	6.302×10^{-3}	2.2×10^{-5} (17.0)	6.28×10^{-3} (0.003)	0.145 b
9.560	2^+	1.410×10^{-1}	2.30×10^{-2} (0.014)	1.18×10^{-1} (0.017)	0.348 b
10.15	3^-	2.960×10^{-1}	2.86×10^{-1} (0.286)	1.00×10^{-2} (0.0024)	91.28 mb
10.57	4^+	1.520×10^{-1}	1.48×10^{-1} (0.40)	4.00×10^{-3} (0.003)	79.88 mb
11.23	4^+	1.970×10^{-1}	7.00×10^{-3} (0.001)	1.90×10^{-1} (0.1)	88.38 mb
11.76	0^+	1.140×10^{-1}	6.30×10^{-3} (0.001)	1.08×10^{-1} (0.01)	13.10 mb

Table 7: Values used to calculate the cross-section and reaction rate using the revised ^{10}Be level scheme[20] for the reaction ^{6}He(α,n)^{9}Be. E_R is the energy of the resonance above the ground state in the compound nucleus ^{10}Be. The Total width, Γ_{TOT}, and the partial widths, Γ_α and Γ_n, are all given in MeV. The spectroscopic factors, C^2S_α and C^2S_α , are given in brackets below the partial widths. The resonant cross-section $\sigma(E_R)$ is also given.

similar.

The large difference between this rate and the rate previously calculated is due to the spectroscopic factor of the entrance channel, C^2S_α, for the 7.542 MeV resonance. The value in Table (7) is 170 times larger than the value in Table (2), as suggested by the recent evaluation of experimental data by Tilley et al. in [20].

However since a fit to the previous rate had already been obtained, it was this rate that was implemented in the r-process simulation. This revised reaction rate calculation is merely included here for completeness. It should be investigated further in future calculations.

5 THE r-PROCESS

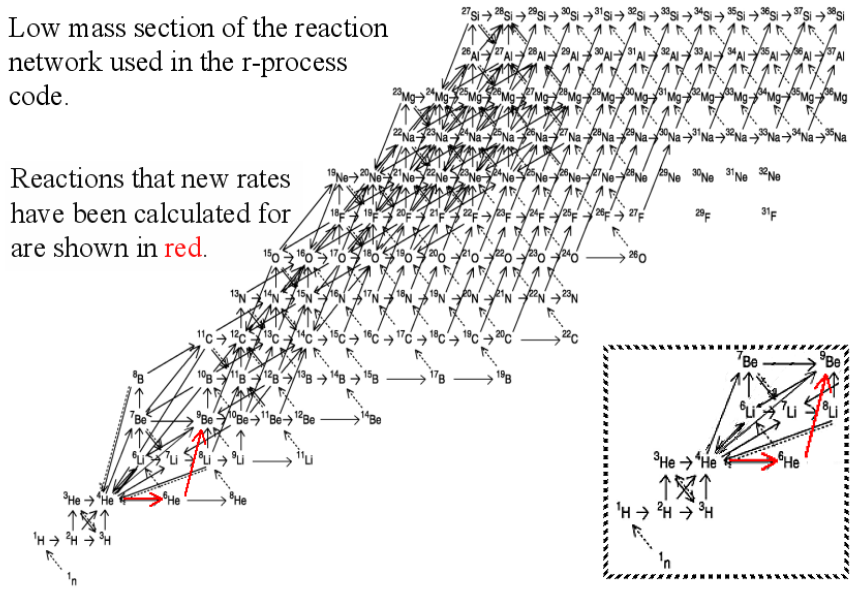

Figure 12: The low mass region of the reaction network used in the r-process simulation. The 2 reactions considered here are shown in red. The inset is an enlargement of the very low mass region.

The r-process is simulated in the neutrino driven wind of a type II supernova. This model of the r-process is derived from a 'realistic' hydrodynamic simulation[7]. The model uses results from a numerical simulation of the neutrino driven wind from [27] to describe the expanding material.

A neutron star is formed by a type II supernova. The proto-neutron star emits a high neutrino flux. Some of these neutrinos heat the outer surface of the proto-neutron star. This causes outward movement of the surface material, called a neutrino driven wind.

The r-process is simulated by a program called RPROC.EXE (see Appendix I for more details). The simulation contains reaction rates for nuclei up to A$\sim$250. The low mass region of the network used in the simulation is shown in Figure (12). The two reactions considered here, ^{4}He(^{2}n,γ)^{6}He and ^{6}He(α,n)^{9}Be, are shown in red in Figure (12).

5.1 THE r-PROCESS SIMULATION AND THEORY

This simulation of the r-process uses an exponential decay model for the temperature of the form

$$T_9 = T_{9i}\ exp\left(\frac{-t}{t_s}\right) + 0.6. \tag{50}$$

Here T_{9i} is the initial temperature in Giga Kelvin (GK) and was set to 9.0 GK, t is the time in seconds, and t_s is the timescale for the temperature decrease and was equal to 0.05s in these simulations.

The reaction rates were calculated per mole, so when the rates are implemented in the code they are multiplied by the particle density, ρ, which is temperature dependent, with

$$\rho = 3.33 \times 10^5 \left(\frac{T_9^3}{s_k}\right) \qquad \text{g cm}^{-3}. \tag{51}$$

Here s_k is the entropy per baryon, where

$$s_k = \frac{s}{k}, \tag{52}$$

s is the entropy, and k is Boltzmann's constant. The entropy per baryon is usually set to a value in the range $50 \leq s_k \leq 400$[22]. In these simulations an intermediate value of 150 was used.

5.2 INVERSE REACTION RATES

Before the reaction rates for the two reactions ^{4}He(^{2}n,γ)^{6}He and ^{6}He(α,n)^{9}Be could be implemented in the code, reaction rates for the inverse reactions, ^{6}He(γ,^{2}n)^{4}He and ^{9}Be(n,α)^{6}He, must also be calculated.

THE INVERSE REACTION RATE OF ^{6}He(α,n)^{9}Be

For a nuclear reaction, $1 + 2 \rightarrow C \rightarrow 3 + 4$, where the particles in the entrance channel (particles 1 and 2) form a resonant state in the compound nucleus C,

which then breaks up into particles 3 and 4, the cross-section can be given by

$$\sigma_{1,2} = \pi\bar{\lambda}^2_{1,2}\frac{2J+1}{(2J_1+1)(2J_2+1)} \times |<3+4|H_{II}|C><C|H_I|1+2>|^2. \quad (53)$$

The cross-section for the inverse reaction is

$$\sigma_{3,4} = \pi\bar{\lambda}^2_{3,4}\frac{2J+1}{(2J_3+1)(2J_4+1)} \times |<1+2|H_I|C><C|H_{II}|3+4>|^2. \quad (54)$$

H_I is the operator describing the entrance channel interaction and H_{II} is the operator describing the interaction in the exit channel[2]. From the principle of time-reversal invariance, the matrix elements of the entrance and exit channels must be identical, therefore

$$|<3+4|H_{II}|C><C|H_I|1+2>|^2 = |<1+2|H_I|C><C|H_{II}|3+4>|^2. \quad (55)$$

Therefore the cross-section ratio of the normal and time-reversed processes is given by

$$\frac{\sigma_{1,2}}{\sigma_{3,4}} = \frac{\bar{\lambda}^2_{1,2}(2J_3+1)(2J_4+1)}{\bar{\lambda}^2_{3,4}(2J_1+1)(2J_2+1)}, \quad (56)$$

$$= \frac{\mu_{3,4}E_{3,4}(2J_3+1)(2J_4+1)}{\mu_{1,2}E_{1,2}(2J_1+1)(2J_2+1)}. \quad (57)$$

The equivalent quantity $\frac{\hbar^2}{(2\mu E)}$ has been substituted in for $\bar{\lambda}^2$, where μ is the reduced mass and E is the centre-of-mass energy.

Using Equation (36) to write expressions for the reaction rates for both the forward and inverse reactions, the ratio of the reaction rates is given by

[2]Usually a factor of $(1+\delta_{1,2})$ is included in the cross-section expression to take into account the doubling of the cross-section for identical particles in the entrance channel. However since neither of the 2 reactions looked at here have identical particles in the entrance channel, the factor has been omitted for the sake of clarity.

$$\frac{<\sigma v>_{3,4}}{<\sigma v>_{1,2}} = \frac{(2J_1+1)(2J_2+1)}{(2J_3+1)(2J_4+1)} \left(\frac{\mu_{1,2}}{\mu_{3,4}}\right)^{\frac{3}{2}} \exp\left(-\frac{Q}{kT}\right), \tag{58}$$

where Equation (25) and the relation $E_{3,4} = E_{1,2} + Q$ (Q>0) have been used.

Therefore the inverse reaction rate of ^{6}He(α,n)^{9}Be is given by

$$< \sigma V >_{n,^9Be} = < \sigma V >_{\alpha,^6He} \left(\frac{1}{8}\right) \left(\frac{24}{9}\right)^{\frac{3}{2}} \exp\left(\frac{-11.605 \times 0.6}{T_9}\right). \tag{59}$$

THE INVERSE REACTION RATE OF ^{4}He(^{2}n,γ)^{6}He

The reaction rate for the inverse reaction of ^{4}He(^{2}n,γ)^{6}He cannot be calculated from Equation (59) since it is a photodisintegration reaction. In a nuclear reaction where $1 + 2 \rightarrow \mathrm{C} \rightarrow 3 + \gamma$, the following expression must be used[1]

$$\frac{<\sigma v>_{3,\gamma}}{<\sigma v>_{1,2}} = \left(\frac{169}{8\pi^5}\right)^{\frac{1}{2}} \frac{(2J_1+1)(2J_2+1)}{3J_3} \left(\frac{\mu\, c^2}{kT}\right)^{\frac{3}{2}} \exp\left(\frac{-Q}{kT}\right). \tag{60}$$

The reaction rate for a photodisintegration reaction should not be multiplied by the particle density, instead it should be multiplied by the photon density, N_γ. The energy distribution of the photons is described by Planck's radiation law, which gives

$$N_\gamma = \frac{8\pi^4}{13c^3h^3}(kT)^3. \tag{61}$$

Therefore the reaction rate multiplied by the photon density is given by

$$N_\gamma < \sigma v >_{3,\gamma} = < \sigma v >_{1,2} \times \left(\frac{2\pi\hbar^2}{\mu kT}\right)^{\frac{-3}{2}} \frac{(2J_1+1)(2J_2+1)}{2J_3+1} \times \exp\left(\frac{-Q}{kT}\right). \tag{62}$$

This gives

$$N_\gamma < \sigma V >_{^6He,\gamma} = < \sigma v >_{^4He,^2n} \times 1.08 \times 10^{20} \times T_9^3 \times 3 \times \exp\left(\frac{-11.269}{T_9}\right) \quad (63)$$

for the ^{6}He(γ,^{2}n)^{4}He reaction.

5.3 THE β-DECAY OF ^{6}He

^{6}He is radioactive, and it decays by beta emission,

$$^6\mathrm{He} \rightarrow {}^6\mathrm{Li} + \mathrm{e}^- + \bar{\nu}. \quad (64)$$

So that ^{6}He is fully included in r-process simulations, its β-decay must be included. The decay constant, λ, is the probability of an atom decaying, per unit time. It is related to the half life, $t_{1/2}$ of the nucleus by the relation

$$\lambda = \frac{\ln 2}{t_{1/2}}. \quad (65)$$

^{6}He has a half-life of 0.8067 s[4].

5.4 THE REACTION RATE OF ^{4}He(αn,γ)^{9}Be

The reaction rate used in the r-process simulation for the reaction ^{4}He(αn,γ)^{9}Be was found to be the rate calculated in [19] and has become outdated. A more recent calculation in [3] was used, which found that the reaction rate was a factor of 2 smaller than the rate in [19]. Therefore the code was altered to reflect this and the reaction rate is now

$$< \sigma v >_{^4He,\alpha n} = \frac{1}{2} \times \frac{2.59 \times 10^{-6}}{T_9^2(1 + 0.344T_9)} \times \exp\left(\frac{-1.062}{T_9}\right). \quad (66)$$

5.5 RESULTS AND DISCUSSIONS

Three different r-process simulations were run, one did not include ^{6}He, the other two included the ^{6}He(α,n)^{9}Be reaction, one of which included the reaction rate

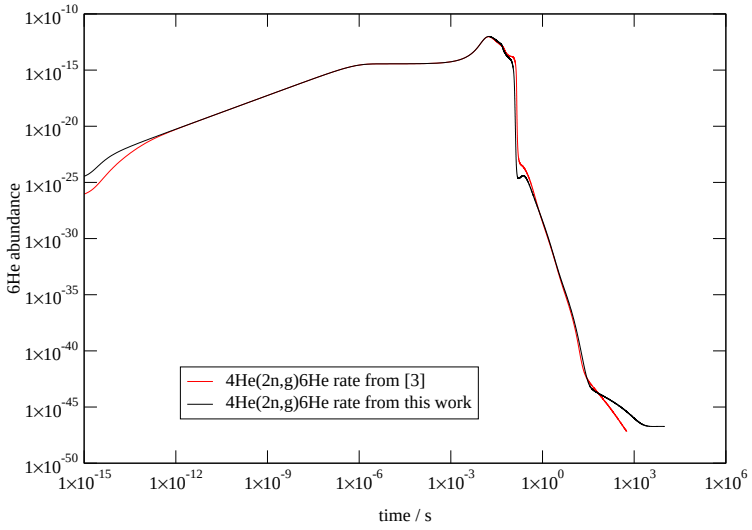

Figure 13: ^{6}He production in r-process simulations against time.

for ^{4}He(2n,γ)^{6}He calculated in [3], and the other included the rate calculated here.

^{6}He PRODUCTION

Figure (13) clearly shows that more ^{6}He is produced in the r-process simulation which included the rate for the reaction ^{4}He(2n,γ)^{6}He calculated in this work. However, Figure (14) shows that at T_9=4, the ^{6}He abundance drops below the ^{6}He abundance curve obtained when the simulation was run for the previous estimate of the reaction rate. This coincides with the temperature at which the reaction rate for ^{6}He(α,n)^{9}Be becomes dominant over the rate of the ^{12}C(n,α)^{9}Be reaction. This is shown in Figure (16), where the reaction rates multiplied by the density, ρ, have been plotted for reactions which produce ^{9}Be. The reaction rates have been multiplied by ρ, since the rates in the r-process simulation are multiplied by ρ. This is therefore more indicative of which reactions are dominant in the simulation. The reverse rate for a reaction is also plotted and is shown by a dashed line of the same colour as for the forward

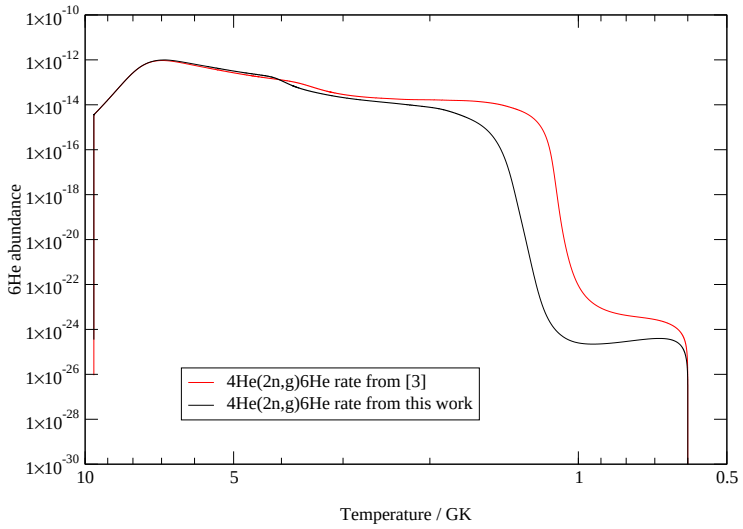

Figure 14: ^{6}He production in r-process simulations against temperature, T_9.

reaction.

The drop in ^{6}He abundance at T_9=4 indicates that the increased ^{4}He(2n,γ)^{6}He rate causes the ^{6}He abundance to be sufficiently large that there is now a flow though the ^{6}He(α,n)^{9}Be reaction towards higher masses.

^{9}Be PRODUCTION

Figure (17) shows a similar drop in abundance for ^{9}Be, at T_9=4, in the r-process simulation which includes the ^{4}He(2n,γ)^{6}He rate calculated here. All three curves plotted in Figure (17) exhibit an increase in abundance between $2 \leq T_9 \leq 3$. The ^{9}Be adundance calculated using the ^{4}He(2n,γ)^{6}He rate calculated here, is consistantly lower than the other 2 curves. This is probably due to the reduced neutron abundance caused by the ^{4}He(2n,γ)^{6}He reaction. Figure (18) shows the neutron abundance against temperature for the three different r-process simulations. The simulation which includes the increased ^{4}He(2n,γ)^{6}He rate, shows a significant reduction in neutron abundance between $0.5 \leq T_9 \leq 3$. This means there are less neutrons available for the ^{4}He(αn,γ)^{9}Be reaction,

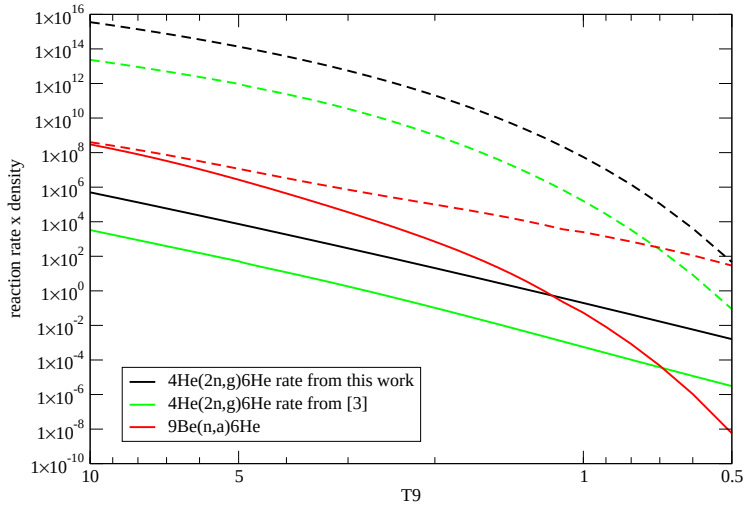

Figure 15: The rates of reactions, in the r-process simulation, which produce ^{6}He. The reaction rates have been multiplied by the density, ρ. Inverse reaction rates are also plotted. The inverse rate is indicated by a dashed line of the same colour as for the forward reaction.

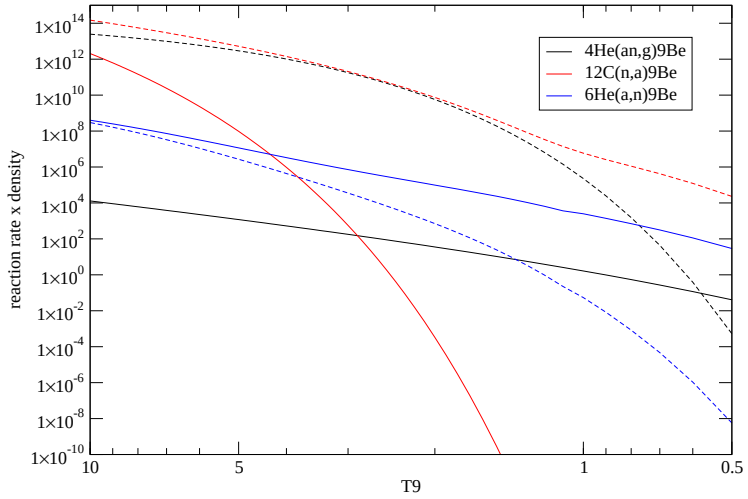

Figure 16: Reaction rates for reactions which produce ^{9}Be. The rates have been multiplied by the density, ρ.

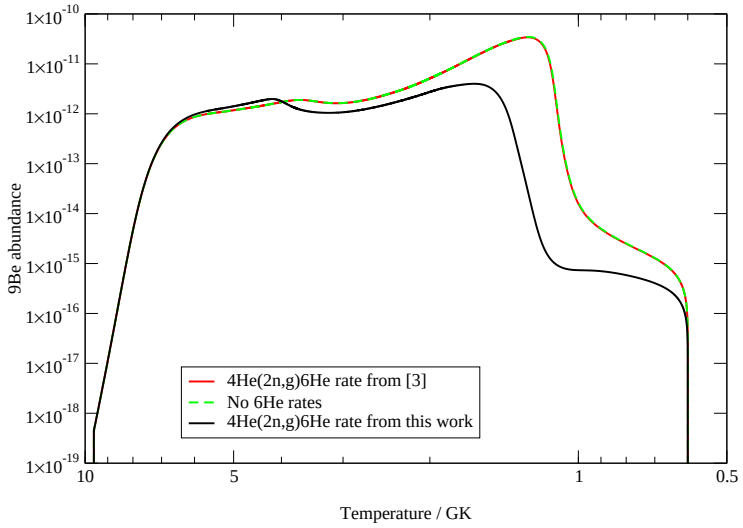

Figure 17: ^{9}Be production in r-process simulations against temperature, T_9.

consequently less ^{9}Be is produced.

^{12}C PRODUCTION

Figure (19) shows the variation in ^{12}C abundance with temperature, during the three r-process simulations. The simulation including the increased ^{4}He(2n,γ)^{6}He rate shows a decrease in abundance after T_9=4 in comparison with the abundance obtained without this reaction. This decrease in adundance is due to the reduced ^{9}Be abundance, since there is less ^{9}Be available for the ^{9}Be(α,n)^{12}C reaction. However there is an increase in abundance for $T_9 \geq 1.5$. This is most likely due to the reduced neutron abundance causing the ^{9}Be(n,α)^{6}He reaction to also be reduced.

FINAL ABUNDANCES

Figure (20) shows the final elemental abundances produced in the 3 different r-process simulations. The curves plotted for the simulation using the ^{4}He(2n,γ)^{6}He rate from [3] and without a ^{4}He(2n,γ)^{6}He rate are identical. The

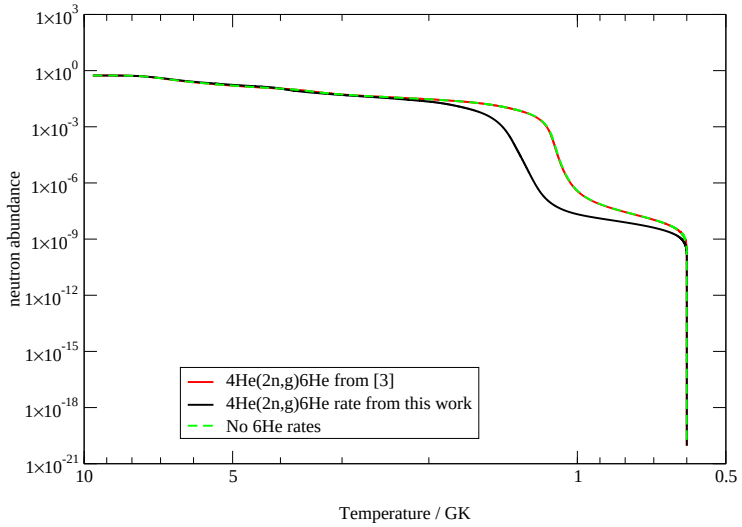

Figure 18: Neutron abundance against time for r-process simulations which include estimates for the ^{4}He(2n,γ)^{6}He rate and for one that does not.

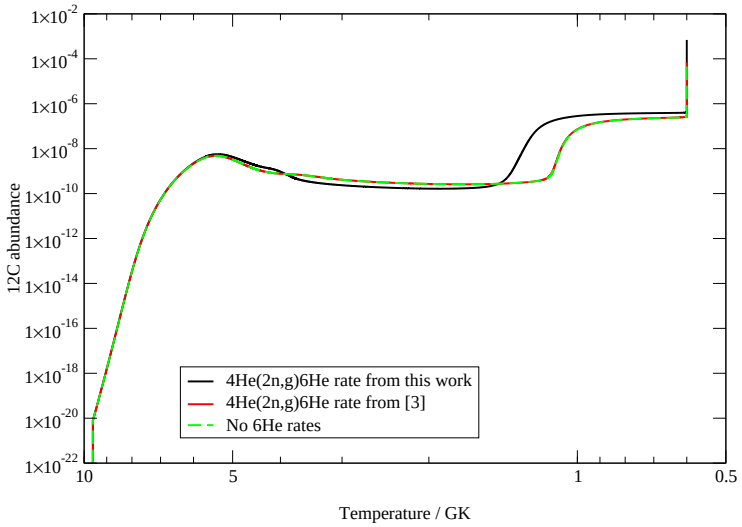

Figure 19: ^{12}C production in r-process simulations against temperature, T_9.

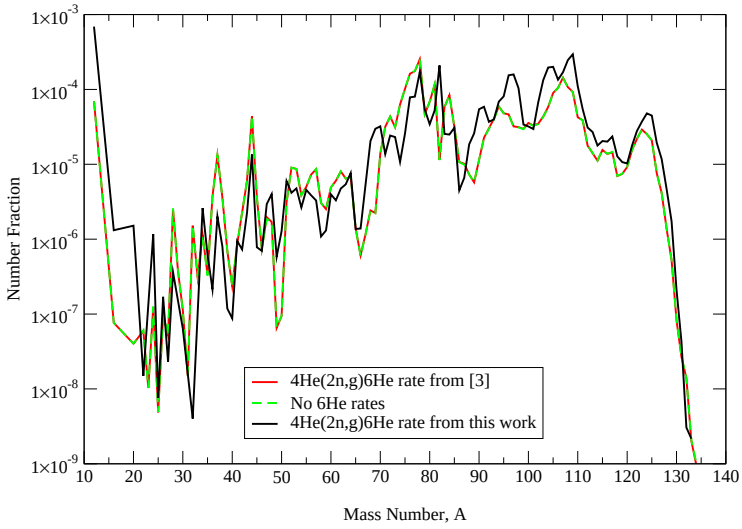

Figure 20: The final elemental abundance curve produced by the r-process simulation. There are three curves plotted, one for the simulation without a ^{4}He(2n,γ)^{6}He rate included, one with the old ^{4}He(2n,γ)^{6}He rate calculated in [3] and one with the ^{4}He(2n,γ)^{6}He rate calculated in this work.

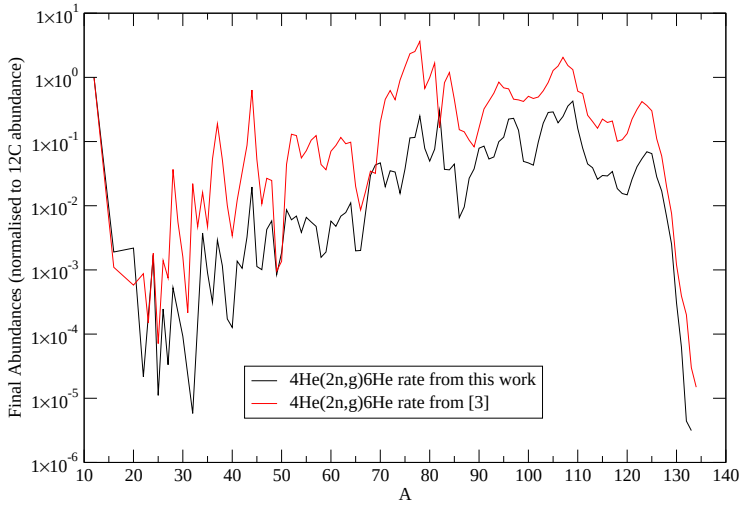

Figure 21: Final abundances against mass number A, normalised to ^{12}C abundance.

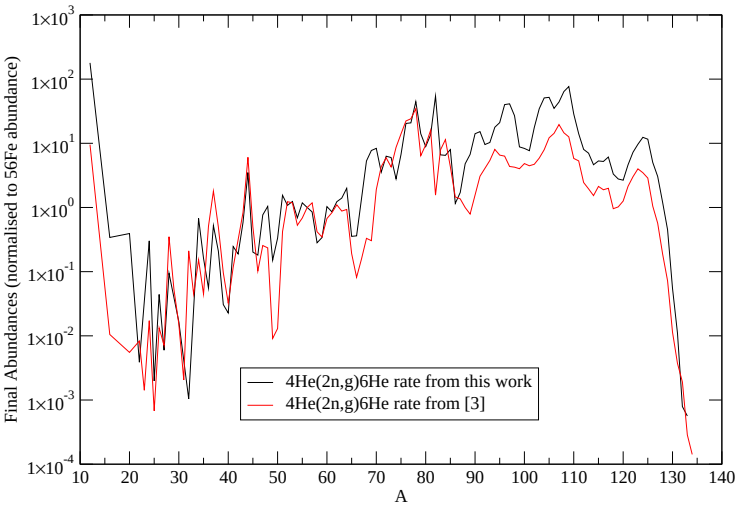

Figure 22: Final abundances against mass number A, normalised to the ^{56}Fe adundance.

curve for the simulation which includes the ^{4}He(2n,γ)^{6}He rate calculated in this work is significantly different from the other two curves. There is a much larger ^{12}C abundance. Nuclei with mass numbers A $\geq$ 85, have generally increased abundances, indicating an increased flow towards heavier nuclei.

Figure (21) shows the abundance curves for the simulation using the ^{4}He(2n,γ)^{6}He rate from [3] and the ^{4}He(2n,γ)^{6}He rate calculated here, normalised to ^{12}C abundance. This shows that, compared with the ^{12}C abundance, there is less of a flow towards heavy nuclei. Figure (22) shows these same two curves normalised to the ^{56}Fe abundance. ^{56}Fe was chosen since this is the last nuclide for which fusion reactions are exothermic, and it is the most stable nucleus, having the highest binding energy per nucleon. The curve plotted for the simulation which included the ^{4}He(2n,γ)^{6}He rate calculated here, shows a consistantly higher abundance for nucei A $\geq$ 56.

The r-process exhibits characteristic peaks at A=80, A=130 and A=195, due to neutron-magic-numbered nuclei stalling the flow toward heavier nuclei.

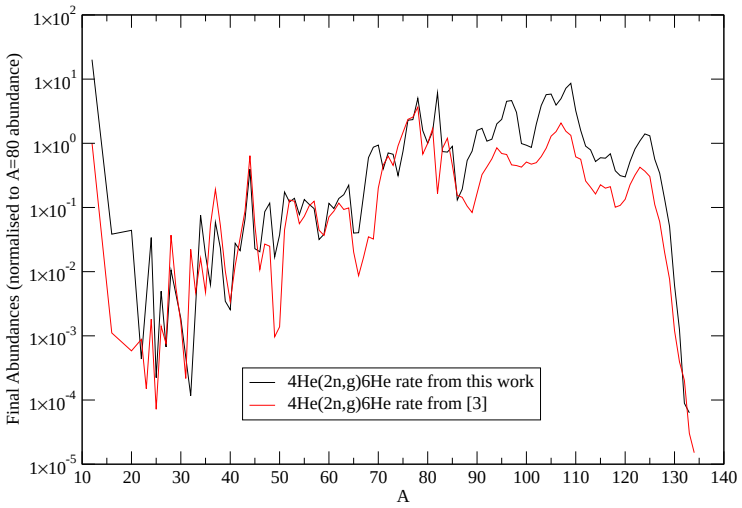

Figure 23: Final abundances against mass number, A, normalised to the r-process abundance peak at A=80.

These simulations of the r-process terminate before A=130 and A=195, due to lack of neutrons, however an increase in abundance around A=80 would be expected. Figure (23), which shows the elemental abundance normalised to the A=80 abundance, was plotted to investigate this. The curve, plotted for the simulation which included the increased ^{4}He(2n,γ)^{6}He rate, shows a similar abundance to that for nuclei A $\geq$ 80, there is no peak visible. The curve, plotted for the simulation with the smaller ^{4}He(2n,γ)^{6}He rate, does exhibit a peak, but it is not pronounced. The un-normalised curves displayed in Figure (20) do show a slight increase in abudance around A=80, however none of the simulations sucessfully replicate the r-process peak at A=80.

Figure (24) shows the percentage of nuclei with mass greater than A. In the mass region 75 $\leq$ A $\leq$ 110, the simulation with the increased ^{4}He(2n,γ)^{6}He rate, clearly has a greater percentage of nuclei with these higher masses. Between 110 $\leq$ A $\leq$ 134 both curves show similar percentages of the heaviest nuclei produced in the simulation. The simulation ran with the ^{4}He(2n,γ)^{6}He rate from [3] has

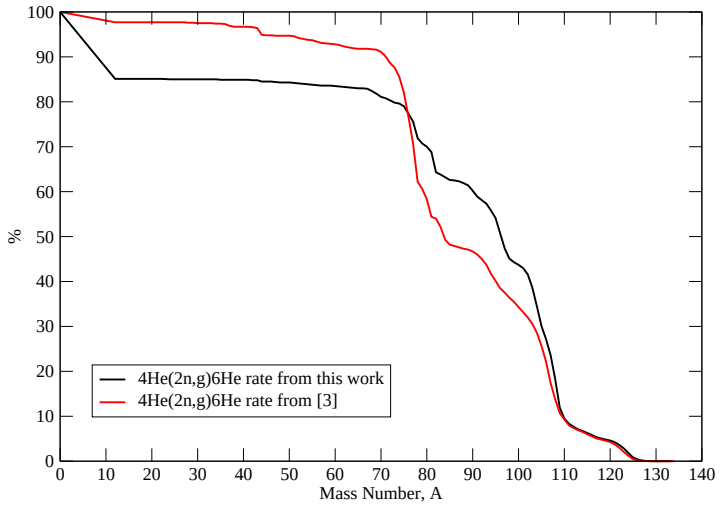

Figure 24: Percentage of nuclei with mass greater than A against A.

50% of nuclei with mass greater than A=83, whereas the simulation with the increased ^{4}He(2n,γ)^{6}He rate, has 50% of it's nuclei with mass great than A=95. This clearly shows that the inclusion of the increased ^{4}He(2n,γ)^{6}He rate in the r-process simulation resulted in an increased flow towards higher masses. However the simulations all terminate at A$\sim$134, so the increased ^{4}He(2n,γ)^{6}He rate did not increase the mass number at which the r-process simulation terminates.

Figure (25) shows the elemental abundance in the region $63 \leq A \leq 134$. The curves have been normalised such that the total number of nuclei in the region is equal to 1. Figure (25) also shows the r-process abundances from [21], which have been normalised in this same manner. There does not seem to be any correlation between the solar system r-process abundances from [21] and the r-process simulation abundances. In fact both simulation curves have a negative correlation coefficient of $\sim$ -0.2 when compared to the solar system r-abundances. This is most likely due to the termination of the simulations at A=134 due to lack of neutrons. Should the simulations be repeated for different environmental conditions such as a shorter timescale, t_s, or higher entropy, s_k,

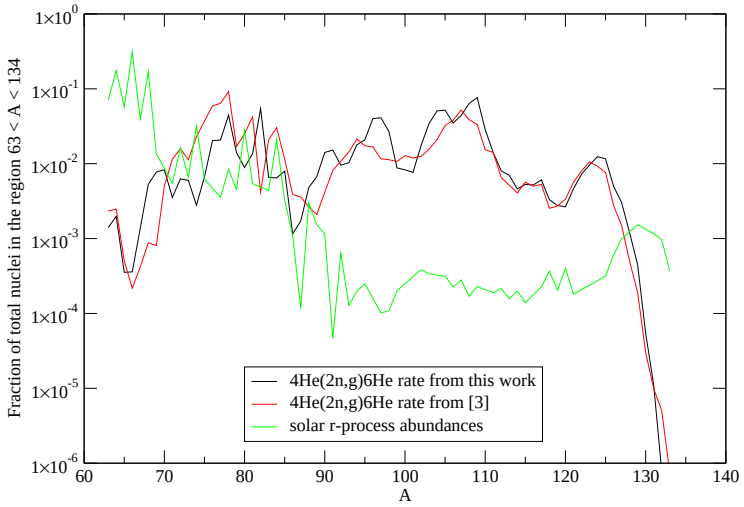

Figure 25: Fractional abundance of nuclei in the region $63 \leq A \leq 134$ against A.

a better fit to the solar system abundances might be obtained.

COMPARISON WITH OTHER R-PROCESS SIMULATIONS

Figure (26) is the final elemental r-process abundance curve published in [7]. This figure was produced using the same r-process simulation that was used in this work. The r-process abundances in Figure (26) provide a better fit to the solar system r-abundances in comparison with the simulations performed for this work. Figure (27) is also from [7]. It shows three different r-process final abundance curves produced for three different timescales, t_s. Plots (b) and (c) in Figure (27) both terminate at $A \sim 135$, like the simulations performed here, however (a) runs sucessfully up to $A \sim 250$. The timescale for this simulation is a factor of 10 smaller than the timescale used in this work. The simulation with the shortest timescale, and therefore the fastest neutrino-driven wind, is successful at producing elements up to $A \sim 250$ since the timescale for expansion is shorter than the neutrino-nucleon collision timescale[7], t_ν. When $t_s < t_\nu$ the

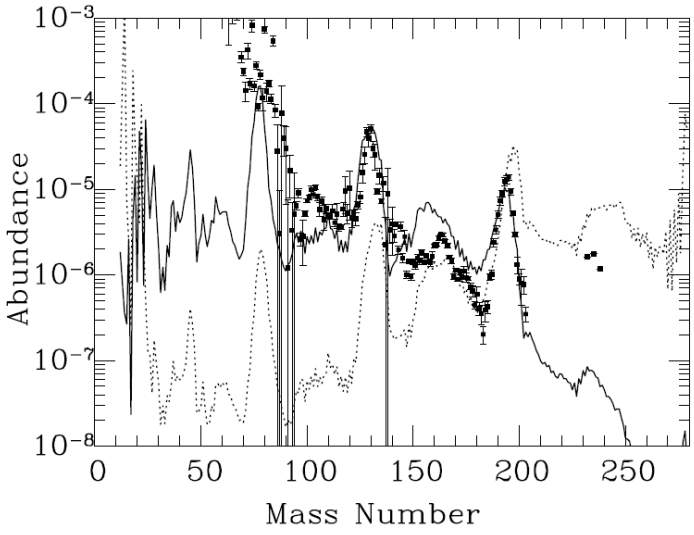

Figure 26: The final r-process abundance curve published in [7]. This curve was produced using the same r-process simulation as used in this work. The black squares indicate the solar r-process abundances from [21]. In [7] the simulation was run for the full reaction network, and a smaller α-network. The solid line indicates the results from the full network. The simulations run for this work were for the full reaction network.

r-process is not hindered by neutrino interaction processes, such as

$$\nu_e + \mathrm{n} \rightarrow \mathrm{p} + \mathrm{e}^-, \tag{67}$$

which reduces the number of neutrons available for the r-process.

Therefore the r-process simulation should be run for a shorter timescale to investigate whether the inclusion of the ^{4}He(2n,γ)^{6}He and ^{6}He(α,n)^{9}Be reactions produces a better fit to the solar system r-process abundances, and increases the mass number at which the simulation terminates.

5.6 CONCLUSION

The inclusion of the enhanced ^{4}He(2n,γ)^{6}He reaction rate resulted in an increased abundance of ^{6}He, enabling the ^{6}He(α,n)^{9}Be reaction to provide a flow towards heavier nuclei. This initially results in an increased ^{9}Be abundance.

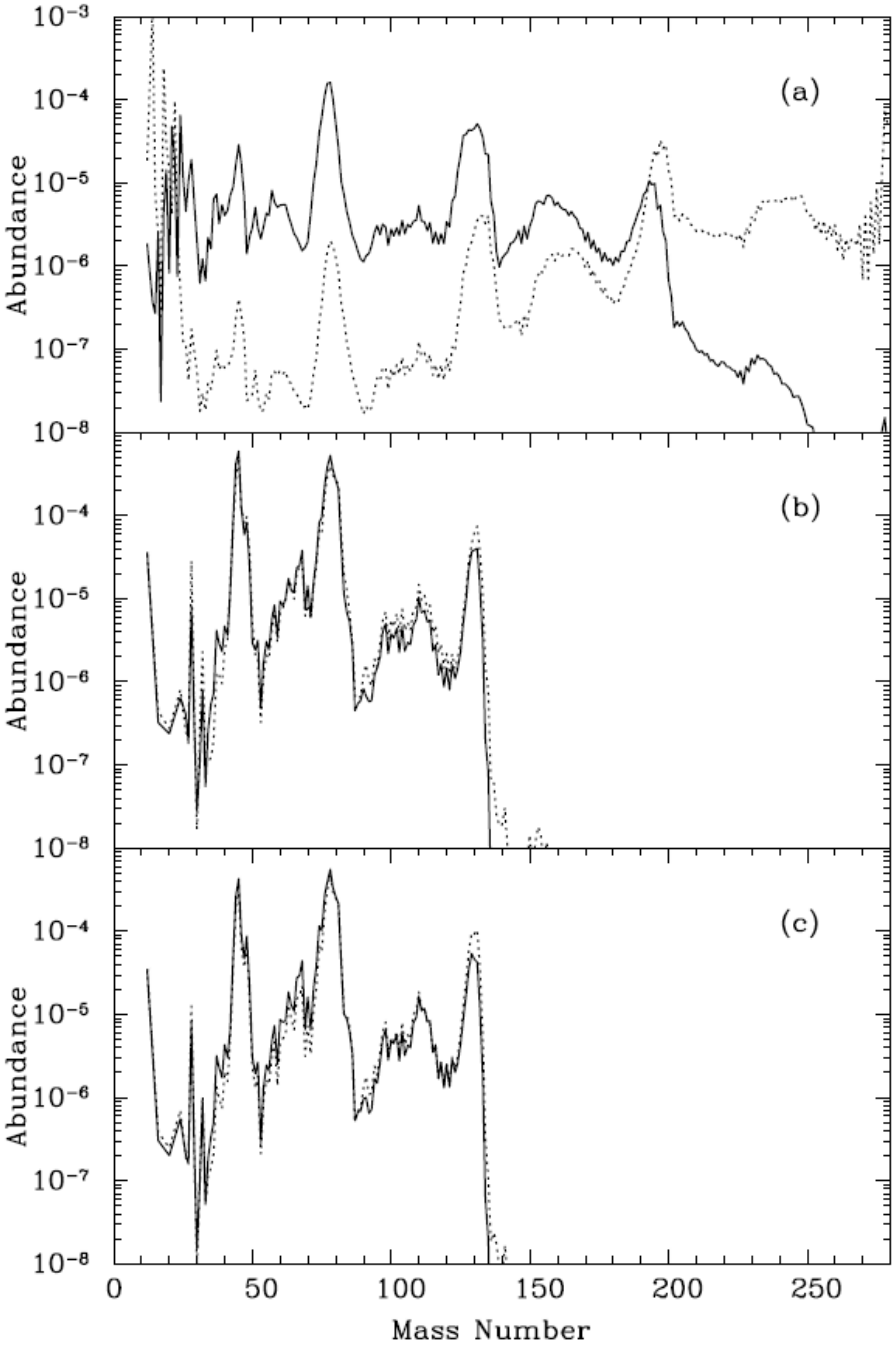

Figure 27: Three final elemental abundance curves from [7]. The simulation was run for three different timescales, t_s = (a) 5.1 ms, (b) 53 ms, and (c) 100 ms. The solid line represents the abundances obtained from the full reaction network that was also used in the simulations performed for this work.

However the ^{4}He(2n,γ)^{6}He reaction burns neutrons and causes a decrease in the neutron abundance, thus reducing the number of neutrons available for the ^{4}He(αn,γ)^{9}Be reaction and resulting in a decreased ^{9}Be abundance. This affects the ^{9}Be(α,n)^{12}C reaction, causing an initial decrease in ^{12}C abundance. However there is an increase in ^{12}C abundance when $T_9 \leq 1.5$, probably due to the decreased neutron abundance reducing the ^{9}Be(n,α)^{6}He rate.

The inclusion of an increased ^{4}He(2n,γ)^{6}He rate also significantly affects the calculated, final elemental abundances. There is an increase in heavier elements. 50% of the nuclei produced by the simulation with the increased ^{4}He(2n,γ)^{6}He rate have a mass, $A \geq 95$, as opposed to $A \geq 83$ for the other 2 simulations which contained either no ^{4}He(2n,γ)^{6}He rate, or included the reduced rate found previously in [3]. It was also found that the inclusion of an increased ^{4}He(2n,γ)^{6}He rate did not reproduce the characteristic r-process peaks, nor reproduce the solar system r-process elemental abundances. However, should the simulation be run for a timescale shorter than the neutrino-nucleon collision timescale, the situation could be vastly improved.

6 FUTURE WORK

The interference in the cross-section in the ^{6}He(α,n)^{9}Be was found to have a negligable affect on the reaction rate. However, the estimate of the interference term in the cross-section was calculated rather primatively. A better estimate of the interference would be obtained by using r-matrix theory to calculate the interference.

The r-process simulations did not run up to very heavy elements. The effect of running the simulations for different environmental conditions, such as higher entropy and a reduced timescale, should be investigated.

7 CONCLUSION

It was hypothesised that the reactions ^{4}He(2n,γ)^{6}He and ^{6}He(α,n)^{9}Be could be very important in simulations of the r-process, in the shock fronts of supernovae. In this model the seed abundance is reassembled from the free α's and nucleons in statistical equilibrium, however this process is hindered by the lack of stable nuclei with mass numbers of 5 and 8. The combination of the ^{4}He(2n,γ)^{6}He reaction with the ^{6}He(α,n)^{9}Be reaction bridges these mass gaps.

The reaction rate for the ^{6}He(α,n)^{9}Be reaction was calculated in a program. An updated energy level scheme for ^{10}Be was used. The temperature dependence of the reaction rate was determined and an exponential function was fitted to the rate.

Two mechanisms by which the ^{4}He(2n,γ)^{6}He reaction can occur are discussed; succesive neutron capture and dineutron capture. Previous estimates of successive neutron capture were found to be insufficient to provide a substantial flow towards heavy nuclei in r-process simulations. An existing program was modified to improve integration accuracy and to reduce run time. Also, more recent input values were entered. It was found that the new resonant successive capture reaction rate estimates were on average 37% larger than the previous ones, but were still the same order of magnitude. The successive neutron direct capture rate was unchanged.

This same program was then adapted to calculate the dineutron capture rate. Both resonant capture and direct capture were investigated. It was found that the dineutron reaction rate was dominated by the direct capture mechanism. The total dineutron reaction rate was was $\sim 2 \rightarrow 3$ orders of magnitude larger than the successive capture rate.

The two reactions ^{4}He(2n,γ)^{6}He and ^{6}He(α,n)^{9}Be were added into an r-process simulation. Three simulation were run. One used the reaction rates calculated in this work, another used a previous (smaller) estimate of the ^{4}He(2n,γ)^{6}He rate, and a third did not contain a ^{4}He(2n,γ)^{6}He rate. It was found that the

larger ^{4}He(2n,γ)^{6}He rate produced significantly more ^{6}He, and caused a decrease in neutron abundance. This had an knock-on effect of reducing the ^{9}Be abundance, as there were fewer neutrons for the ^{4}He(αn,γ)^{9}Be reaction. This in turn caused an initial decrease in ^{12}C abundance. However the decrease in neutron abundance caused a decrease in the ^{9}Be(n,α)^{6}He rate, causing an enhanced ^{12}C abundance for $T_9 \leq 1.5$.

The inclusion of these 2 reactions also resulted in an increased flow towards heavier nuclei. 50% of the nuclei produced in the simulation with the increased ^{4}He(2n,γ)^{6}He rate had a mass ≥ 95. This compares with 50% of the nuclei in the other 2 simulations having $A \geq 83$. However the increased ^{4}He(2n,γ)^{6}He rate did not cause a better reproduction of the r-process characteristic peaks, nor did it better replicate the r-process solar abundances. This situation would most likely be improved by running the simulations for higher entropy and a timescale less than the neutrino-nucleon collision timescale.

8 APPENDIX I: PROGRAM INDEX

8.1 RATE

RATE is an almost entirely new FORTRAN77 program, written to calculate the ^{6}He(α,n)^{9}Be rate. It contains the following files:

- rate1.f
- func.f
- func2.f
- func3.f
- pene2.f
- coull.f

This program also requires the libraries libmathlib.a and libkernlib.a from the CERN library, so that the subprogram DGAUSS can be used to perform the integration.

The main program is contained in the file rate1.f, this is where all the input is read into the program. The file func.f contains the function func, which is the function integrated by DGAUSS. In this function the cross-section for the reaction is calculated. The files func2.f and func3.f contain the functions func2 and func3 which calculate the cross-section with the addition of interference terms and subtraction of interference terms respectively. The program automatically looks through the input data for each of the resonances in the compound nucleus, to find which levels have the same spin. No parity data for the resonances is input, the program assumes that energy levels with the same spin have the same parity.

8.2 TWOSTEP

The program TWOSTEP was originally used in [3] to calculate the successive capture of 2 neutrons on ^{4}He. This version of TWOSTEP and all the variations of this program are FORTRAN77 programs. I modified this program so that the integration was performed by an external subprogram from the cern library called DGAUSS. DGAUSS uses adaptive Gaussian quadrature to calculate the

double integral in Equation (48). This equation is of the form

$$I = \int_{x_1} f(x_1) \left[\int_{x_2} f(x_1, x_2) dx_2 \right] dx_1. \tag{68}$$

The TWOSTEP program previously used a version of the trapezium rule to calculate the integrals. This program consists of the following files:

- twostep2.f
- sub2.f
- total2.f
- rate1.f
- all2.f
- coull.f
- rate4.f
- bshift.f

and requires the libraries libmathlib.a and libkernlib.a from the CERN library so that the subprogram DGAUSS can be called.

The main body of the program is contained in twostep2.f. The files coull.f and bshift.f calculate penetrabilities and transmission values so that the integrands in Equation (48) can be calculated. The file rate1.f is $f(x_1, x_2)$ in Equation (68), sub2.f calls rate1.f, and rate4.f integrates the function sub contained in sub2.f. These three files calculate the section of Equation (68) contained in the square brackets. Also in rate4.f, the bracketed integral is multiplied by $f(x_1)$. This subroutine is called by the function all in all2.f. The function all is then integrated by the subroutine total, contained in the file total2.f. The main program calls the total subroutine and then reads the temperature and reaction rate out to the screen and to an output file called twostep.dat.

TWOSTEP INPUT DATA

The first step in the reaction ^{4}He(2n,γ)^{6}He is the the first neutron capture on ^{4}He to form the unbound ^{5}He. The program asks that the charges, Z, and the mass numbers, A, of the target and projectile nuclei be entered. The neutron is the projectile, therefore AP=1 and ZP=0. The target nucleus is ^{4}He, where AT=4 and ZT=2. The program then asks for the resonance energy, which in

this case is 0.9 MeV and the relative angular momentum between the target and projectile. A spectroscopic factor of 0.51 is entered. Then the spins of the resonance, $\frac{3}{2}$, the target, 0, and the projectile, $\frac{1}{2}$, are input.

In the second step of the reaction, the capture of a second neutron onto ^{5}He, the neutron is the projectile and the ^{5}He is the target nucleus. Therefore AP=1, ZP=0, AT=5 and ZT=2. A resonant state in ^{6}He is formed, which can decay either by γ-decay or 2-neutron emission. The energy of the resonance in ^{6}He is 1.797 MeV above the ground state. The 2 neutron separation energy, s2n, is 0.973 MeV. The energy of the emitted γ-photon is 1.797 MeV, and the γ-decay width is 9.88×10^{-12} MeV. The multipolarity of the decay-transition is 2, and the photon carries away 1 unit of angular momentum. A spectroscopic factor of 0.5 is then input. The 2-neutron decay width is then asked for, which is 0.113 MeV. The charge on the emitted dineutron is 0. The spin of the resonance is 2, the target is $\frac{3}{2}$ and the projectile is $\frac{1}{2}$. The the spin of an emitted dineutron is 0.

8.3 TWOSTEP2

The program TWOSTEP2 is a variation on TWOSTEP. I modified the code so that the dineutron capture rate on ^{4}He could be calculated. The dineutron formation cross section was added into the code by finding a functional fit to the experimental cross-section. (See Appendix III.) The program TWOSTEP2 consists of the following two CERN libraries; libmathlib.a and libkernlib.a as well as:

- 2ntwostep2.f
- 2nsub2.f
- 2ntotal2.f
- 2nrate1.f
- all2.f
- coull.f
- 2nrate4.f
- bshift.f

These files and the functions and subroutines contained there in, perform the

same tasks as their namesakes in the TWOSTEP program (see section above). The output is written to the screen and to a file called twostep2.dat.

TWOSTEP2 INPUT DATA

The first step in the reaction ^{4}He(^{2}n,γ)^{6}He, is the formation of the dineutron. The program asks for the mass number, A, and charge, Z, of the projectile and target nuclei. In this case the projectile and target nuclei are the same with AT=AP=1, and ZT=ZP=0. The program then asks for the resonance energy, since the dineutron cross-section is being treated as a resonance at zero energy, the resonance energy is zero. The program asks for the change in angular momentum, L, of the reaction, which is also zero. A spectroscopic factor of zero is then entered, followed by the spin of the resonance, which is zero. The program then asks for the spins of the projectile and target nuclei, in this case JT=JP=0.5. Then limits and a required accuracy are requested for the integration of the first step, in this case the limits ran from 0 to 25, and an accuracy of 1×10^{-30} was used.

The second step in the reaction is the dineutron capture on ^{4}He. This time, AT=4, ZT=2, AP=2, ZP=0 is entered. The resonance energy of the resonant state in ^{6}He, 1.797 MeV, is entered. The 2 neutron separation energy is entered, 0.973 MeV. The energy of the emitted γ-photon is entered, and the γ-width and the multipolarity of the transition is asked for. The γ-energy is equal to the energy of the resonance, 1.797 MeV. The width=9.88 μeV, and the multipolarity is equal to 2. The spin of the resonance, 2, is entered, followed by the spins of the target and projectile nuclei, which is zero for both. The two neutron resonance width is aked for, and is equal to 0.113 MeV. The angular momentum change of the reaction is 2. The same integration limits, and accuracy, were used for the second step as were used for the first.

8.4 TWOSTEPDC

This version of the program TWOSTEP calculates the reaction rate for dineutron direct capture on ^{4}He. The direct capture cross-section was calculated in a program called JEZEBEL, and a functional fit was found (See Appendix III), and this was added into the program. TWOSTEPDC contains the following files:

- 2ndctwostep2.f
- 2ntotal2.f
- dcall2.f
- 2nrate4.f
- 2ndcsub6.f
- 2nrate1.f
- coull.f
- bshift.f

These files perform the same tasks as their namesakes in the original TWOSTEP program. This program also requires the libraries libmathlib.a and libkernlib.a from the CERN library.

TWOSTEPDC INPUT PARAMETERS

As in TWOSTEP2, the first step in the reaction ^{4}He(^{2}n,γ)^{6}He, is the formation of the dineutron. Consequently all the input parameters are the same as those described for TWOSTEP2, apart from the integration limits and accuracy. The limits used were 0 to 1 MeV and an accuracy of 1×10^{-6}.

The second stage, the direct capture of the dineutron on ^{4}He, also requires the same input parameters as TWOSTEP2. The same values as described for the TWOSTEP2 program were used except the limits and the accuracy. The same limits and accuracy were used in this step as were used in the first step of the TWOSTEPDC program.

8.5 JEZEBEL

JEZEBEL is the program used to calculate the direct capture cross-section for the ^{4}He(^{2}n,γ)^{6}He reaction. The direct capture cross section was also calculated

by Mengoni, as in [25], and the JEZEBEL cross-section was scaled down to match the Mengoni cross-section.

JEZEBEL calculates the direct capture cross-section using a Woods-Saxon potential. There are no analytical solutions for the Woods-Saxon potential like there are for a square-well. Consequently, numerical integration is performed to obtain the wave function. The wave function must be zero at the centre of the well, R=0. Therefore JEZEBEL adjusts the well-depth until the wave function vanishes at R=0. This is the solution when the principal quantum number of the final state is 1. If the principal qunatum number of the final state is > 1, the well depth must be increased further until a wave function is found with a number of zero crossings numerically equal to the principal quantum number of the final state.

JEZEBEL INPUT

JEZEBEL requires the mass and charge of the target and projectile nuclei to calculate the direct capture cross-section. In the case of dineutron capture on ^{4}He, the dineutron is the projectile, MP=2 and ZP=0, and ^{4}He is the target nucleus, AT=4 and ZT=2. The Q-value of the reaction is also required, which in this case: Q-value=0.9 MeV. The spins of the target and projectile nuclei, as well as the spin of the final state, is necessary input. Both the projectile and target, the dineutron and ^{4}He respectively, are spin zero particles, and the spin of the final state, the ground state of ^{6}He, is also zero. The angular momentum carried away by the emitted γ-decay photon is also input. JEZEBEL also requires that the radius and diffuseness of the potential well be entered.

JEZEBEL requires some input relating to how it calculates the wave function in the potential well. Firstly it requires that a guess value for the well depth is entered, in this work a guess of 2 MeV was used. JEZEBEL also requires a number of mesh points and a mesh size in femto-metres to be entered. The mesh point number and mesh size determines where and how often the numerical integration is performed to obtain the wave function. In this work 200 mesh

points were used, with a spacing of 0.5 fm. This means that the numerical integration was performed at 100 fm and then every 0.5 fm until the centre of the well is reached. For the ^{4}He(^{2}n,γ)^{6}He reaction, JEZEBEL calculated an optimal well depth of 13.078 MeV.

JEZEBEL OUTPUT

JEZEBEL reads out all the input values used in the calculation, and the calculated direct capture cross-section to an external file. The user is asked to give a name for the file, and it is created in the same directory as the program.

8.6 RPROC.EXE

rproc.exe is the program used to simulate the r-process, it is sometimes referred to as rpcode. This program is written in FORTRAN90. Figure (28) shows all the files, subroutines and functions contained in the program. The exponential temperature decay of the simulations (Equation (50)) is written into the subroutine called therm. The density dependence of the simulations (Equation (51)) is also written into this subroutine.

All the reactions considered in this work are low mass and are therefore contained in the file spcompt4.full.f. The only other code altered for this work was the file rebetar3.f, to include the β-decay of ^{6}He, and the main program remain5.f was altered so that that reaction rate coefficients for the reaction ^{6}He(α,n)^{9}Be could be read into the program, and so that the abundance of ^{6}He was read out into data files.

INPUT

The program requires to be in a directory called code, and that there are 2 folders in the same directory as code, one called NACRE, the other called grantdat. Both these folders contain input files for RPROC.EXE. The grantdat directory contains the following files:

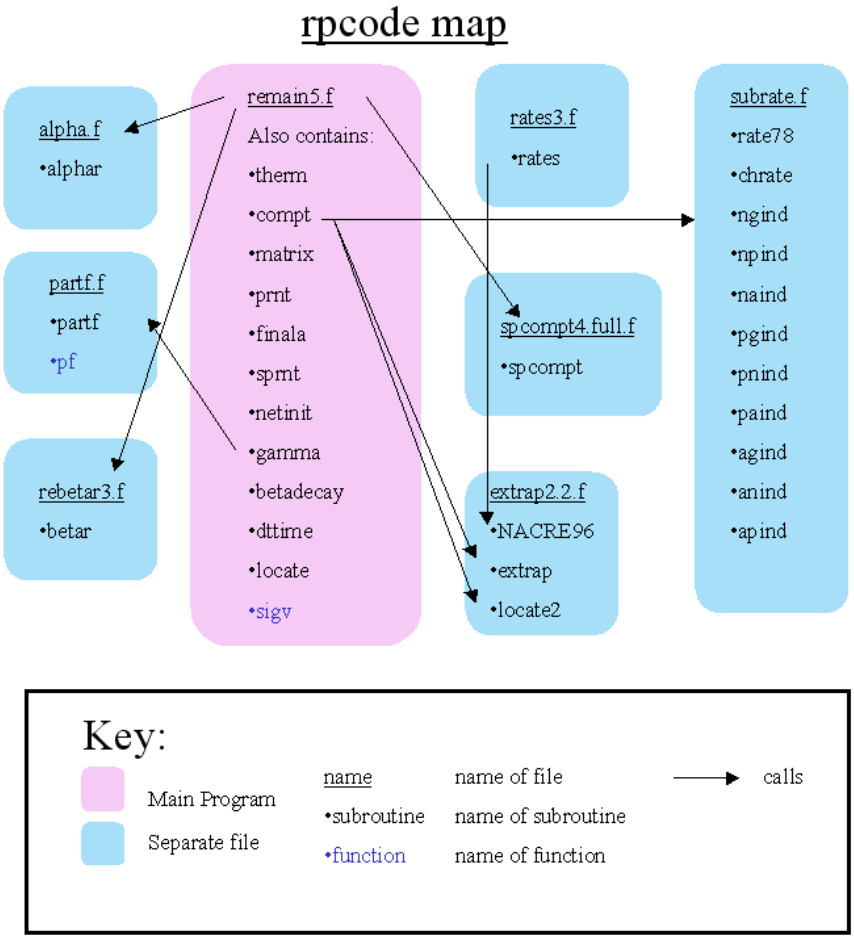

Figure 28: A diagram mapping the different subroutines and functions of the program rproc.exe, also known as rpcode.

- an.rate
- init
- klap.dat
- na.rate
- noemit
- sigmav2
- table

The file an.rate contains data relating to (α,n) reactions on different nuclei. The file contains 13 columns, columns 2 to 4 contain the number of protons, neutrons and nucleons in the nucleus of the target nucleus, and the last 7 columns contain coefficients that describe the reaction rate. The coefficients, a_1 through to a_7, go into a standard equation of the form

$$<\sigma v>_{fit} = \exp\left(a1 + \frac{a2}{x} + a3x^{-\frac{1}{3}} + a4x^{\frac{1}{3}} + a5x + a6x^{\frac{5}{3}} + a7\log(x)\right). \quad (69)$$

The file na.rate contains the same data as na.rate except for (n,α) reactions.

The folder NACRE contains reaction rate data obtained from the Nuclear Astrophysics Compilation of REaction rates. There is a file for each reaction for which NACRE data was used, these files (and their reactions) are:

- 16Can19O
- 17Can20O
- 17Cng18C
- 17Nan20F
- 18Can21O
- 18Cng19C
- 18Nan21F
- 19Can22O
- 19Cng20C
- 19Nan22F
- 19Nng20N
- 20Can23O
- 20Nng21N
- 20Oan23Ne
- 21Nng22N
- 21Oan24Ne
- 22Fan25Na
- 22Nng23N
- 22Oan25Ne
- 22Ong23O
- 23Fan26Na
- 23Oan26Ne
- 23Ong24O
- 24Fan27Na
- 24Fng25F
- 24Oan27Ne

- 25Fan28Na
- 26Fan29Na
- 27Fan30Na
- 25Fng26F
- 26Fng27F

An alteration to the program to include the reaction rate for the ^{6}He(α,n)^{9}Be reaction means an additional input file containing reaction rate coefficients is needed. This file is called fit2.dat, and should be in the same directory as the program.

OUTPUT

The program requires that a directory called test be in the same directory as the program. The program reads data out to various files it creates in that folder. The program creates the following output files:

- final1
- atime1
- aout1
- ztime1
- small1
- burnt1
- netwout1
- carbon12.dat

The file final1 contains the final elemental abundances and contains 4 columns of data:

- 1: Nuclear charge, Z.
- 2: Mass number, A.
- 3: Elemental Abundance.
- 4: Elemental Abundance multiplied by A.

The output file carbon12.dat contains the abundances of light nuclei, the file contains 9 colums:

- 1: Time in seconds.
- 2: Temperature in Giga Kelvin.
- 3: Neutron abundance.
- 4: ^{3}He abundance.
- 5: ^{4}He abundance.
- 6: ^{6}He abundance.

- 7: ^{6}Li abundance.
- 8: ^{9}Be abundance.
- 9: ^{12}C abundance.

The program also reads out data into files in the same directory as itself, these files have the prefixs time, fort and fij. There is also an output file called lightn.dat. It contains most of the same data as carbon12.dat.

9 APPENDIX II: RATE CODE

The program rate, which was used to calculate the ^{6}He(α,n)^{9}Be rate, was mostly written by myself, so the code for this program is included here: (Excluding the subroutine coull and the function pene2, since these were not written by myself.)

9.1 THE MAIN PROGRAM

```
C——Modified Amy Bartlett 11/12/2003 ——
      implicit real*8 (a-h,o-z)
      common /MandZ/at1,zt1,ap1,zp1,r1,at2,zt2,ap2,zp2,Temp,amu
      common /energy/Er(10),EaR(10),EnR(10),Gammar(10),TnR(10),TaR(10)
      common /width/C2Sn(10),C2Sa(10),Gamman(10),Gammaa(10),sigmar(10)
      common /crosssection/ csec(10)
      common /integer/n
      common/angmon/ Ln(10),L(10),La(10)
      common/flag/k,k2
      common/interference/ m(10,10,10)
      common/identifier/ number(10)
      character*10 name
      external func, func2, func3

      write(6,*)'Hello! I calculate reaction rates.'
      write(6,*)'What is your name?'
      read(5,*)name
      write(6,*)'Hello ',name

      open(11, FILE='matrix.out')
      open(10, FILE='func.out')
      open(12, FILE='rate.out')
      open(13, File='sigma.out')
      open(16, File='sigma2.out')
      open(14, FILE='matrix2.out')
      open(15, FILE='ones.out')
      open(17, FILE='delta1.out')
      open(18, FILE='delta2.out')
      open(19, FILE='mmm.out')
      open(20, FILE='m1.out')
      open(21, FILE='m2.out')
      open(22, FILE='m3.out')
      open(23, FILE='m4.out')
      open(24, FILE='m5.out')
      open(25, FILE='delta3.out')
      open(26, FILE='delta4.out')

      write(6,*)'Are you ready to calculate some reaction rates?'
      write(6,*)'y=1, n=0'
```

```
read(5,*)s
IF (s.EQ.0) GOTO 200

a=0
b=10
eps=1.0
hbar=6.5822D-16
eamu=931.502
sol=2.998*(10.0**8.0)
k=0

write(6,*)'Please enter the following information about'
write(6,*)'the entrance channel:'
write(6,*)' '
write(6,*)'Mass of target nucleus (A):'
read(5,*)at1
write(6,*)'Charge on taget nucleus (Z):'
read(5,*)zt1
write(6,*)'Mass of projectile (A):'
read(5,*)ap1
write(6,*)'Charge on projectile (Z):'
read(5,*)zp1
write(6,*)' '

r1=1.3
amu=(at1*ap1)/(at1+ap1)
pi=3.141592654
AvNo=6.02217D19
bk=8.6117D-05
bkMeV=8.6171D-11

write(6,*)'Please enter the following information about'
write(6,*)'the exit channel:'
write(6,*)' '
write(6,*)'Mass of target nucleus (A):'
read(5,*)at2
write(6,*)'Charge on target nucleus (Z):'
read(5,*)zt2
write(6,*)'Mass of projectile:'
read(5,*)ap2
write(6,*)'Charge on projectile (Z):'
read(5,*)zp2

write(6,*)' '
write(6,*)'How many energy levels does the intermediate'
write(6,*)'nucleus have?'
read(5,*)n

DO i=1,n
  write(6,*)'Please enter the following information about'
  write(6,*)'energy level number ',i,':'
```

```
write(6,*)' '
write(11,*)'values for energy level number',i,':'
number(i)=i
write(6,*)'Energy in MeV above ground state:'
read(5,*)ER(i)
write(11,*)'Energy of resonance: ',ER(i)
EaR(i)=ER(i)-7.4104
write(11,*)'Alpha energy: ',EaR(i)
EnR(i)=ER(i)-6.8120
write(11,*)'Neutron Energy: ',EnR(i)
write(6,*)'J:'
read(5,*)L(i)
write(11,*)'J of state: ',L(i)
write(6,*)'L entrance channel:'
read(5,*)La(i)
write(11,*)'Ang Mom change, entrance channel: ',La(i)
write(6,*)'L exit channel:'
read(5,*)Ln(i)
write(11,*)'Ang Mom change, exit channel: ',Ln(i)
E1=EaR(i)
call pene(E1,La(i),at1,zt1,ap1,zp1,TaR(i))
write(11,*)'Alpha Transmission: ',TaR(i)
E2=EnR(i)
call pene(E2,Ln(i),at2,zt2,ap2,zp2,TnR(i))
write(11,*)'Neutron Transmission: ',TnR(i)
write(6,*)'Spectroscopic factor for the entrance channel:'
read(5,*)C2Sa(i)
write(11,*)'Entrance Spectroscopic factor: ',C2Sa(i)
write(6,*)'Spectroscopic factor for the exit channel:'
read(5,*)C2Sn(i)
write(11,*)'Exit Spectroscopic factor: ',C2Sn(i)
write(6,*)'Alpha width:'
read(5,*)gammaa(i)
write(6,*)'Neutron width:'
read(5,*)gamman(i)
gammar(i)=gammaa(i)+gamman(i)
write(11,*)'Alpha resonance width: ',gammaa(i)
write(11,*)'Neutron Resonance width: ',gamman(i)
write(11,*)'Total Resonance width: ',gammar(i)
omega=2.0*La(i)+1.0
restrength=(C2Sa(i)*TaR(i)*C2Sn(i)*TnR(i))/gammar(i)
omgam=omega*restrength
omgam=omgam*10**-6.0
xmu=(at1*ap1)/(at1+ap1)
wave=(hbar*10.0**-6.0)
wave=wave*sol
write(11,*)wave,xmu
wave=wave/DSQRT(2.0*xmu*eamu*EaR(i))
wave=wave*100
sigmar(i)=pi*(wave**2.0)*omega*gamman(i)*gammaa(i)
```

```
      sigmar(i)=sigmar(i)/((gammar(i)/2.0)**2.0)
      write(11,*)'Resonant Cross Section: ',sigmar(i),wave
      write(11,*)' '
    END DO

    write(6,*)'Do you want to include interference terms'
    write(6,*)'in the calculation? (y=1,n=0)'
    read(5,*)k2

    IF(k2.EQ.0) GOTO 236

    IF(k2.EQ.1) THEN
      DO i=1,n
        DO j=1,n
          IF(L(j).EQ.L(i)) m(i,j,L(j))=1
          IF(m(i,j,L(j)).EQ.m(j,i,L(j))) m(i,j,L(j))=0.0
        END DO
      END DO
    END IF

    DO i=1,10
      DO j=1,10
        DO kk=1,10
          IF(m(i,j,kk).EQ.1.0) THEN
            write(6,*)'There is interference between energy level'
            write(6,*)'number ',i,' and energy level number ',j
            write(6,*)'which both have the same spin of ',kk
          END IF
        END DO
      END DO
    END DO

236 write(6,*)'here'

    write(6,*)'k =',k
    DO jj=1,1000
      x=jj*0.01+0.0016
      y=x
      z=func(x)
      write(10,*)y,z
    END DO

    k=1.0

    write(6,*)'Do you want to run this program for a specific'
    write(6,*)'temperature, or a range of temperatures?'
    write(6,*)'(specific=0, range=1)'
    read(5,*)mm
    IF(mm.EQ.0) GOTO 100
    IF(mm.EQ.1) GOTO 300
100 write(6,*)'Please enter a temperature in GK:'
    read(5,*)Temp9
```

```
      Temp=Temp9*10**9.0
      aint=DGAUSS(func,a,b,eps)
      write(6,*)'For T9= ',Temp9,'rate =',aint
      aint2=DGAUSS(func2,a,b,eps)
      write(6,*)'+ interference rate =',aint2
      aint3=DGAUSS(func3,a,b,eps)
      write(6,*)'- interference rate =',aint3
      write(12,900)Temp9,aint !,p
900   format (D25.13,D25.13) !D20.13)

      write(6,*)'Would you like to run the program for a different'
      write(6,*)'temperature (GK) (y=1/n=0)?'
      read(5,*)q
      IF (q.EQ.1) GOTO 100
      IF (q.EQ.0) GOTO 200

300     write(6,*)'Please enter minimum and maximum temperatures in GK:'
      read(5,*)T9min, T9max
      write(6,*)'how many data points would you like?'
      read(5,*)num
      step=(T9max-T9min)/num
      write(6,*)'The step size is ',step,' GK'

      DO j=0,num
        T9=T9min+(j*step)
        Temp=T9*10**9
        aint=DGAUSS(func,a,b,eps)
        aint2=DGAUSS(func2,a,b,eps)
        aint3=DGAUSS(func3,a,b,eps)
        write(12,800)T9,aint,aint2,aint3
800     format (D25.13,D25.13,D25.13,D25.13)
      END DO

      write(6,*)'see rate.out for results!'

200   write(6,*)'Thank you for using this program.'
      write(6,*)'Please use it again soon.'
      write(6,*)'Goodbye ',name,'!'

      DO i=1,n
        write(14,*)'values for energy level number',i,':'
        write(14,*)'Energy of resonance: ',ER(i)
        write(14,*)'Alpha energy: ',EaR(i)
        write(14,*)'Neutron Energy: ',EnR(i)
        write(14,*)'Total Resonance width: ',gammar(i)
        write(14,*)'J of state: ',L(i)
        write(14,*)'Ang Mom change, entrance channel: ',La(i)
        write(14,*)'Ang Mom change, exit channel: ',Ln(i)
        write(14,*)'Alpha Transmission: ',TaR(i)
        write(14,*)'Neutron Transmission: ',TnR(i)
        write(14,*)'Entrance Spectroscopic factor: ',C2Sa(i)
```

```
      write(14,*)'Exit Spectroscopic factor: ',C2Sn(i)
      write(14,*)'Alpha resonance width: ',gammaa(i)
      write(14,*)'Neutron Resonance width: ',gamman(i)
      write(14,*)'Resonant Cross Section: ',sigmar(i)
      write(14,*)' '
    END DO

    DO i=1,10
      DO j=1,10
        DO nn=1,5
          IF(nn.EQ.1) write(20,*)i,j,nn,m(i,j,1)
          IF(nn.EQ.2) write(21,*)i,j,nn,m(i,j,2)
          IF(nn.EQ.3) write(22,*)i,j,nn,m(i,j,3)
          IF(nn.EQ.4) write(23,*)i,j,nn,m(i,j,4)
          IF(nn.EQ.5) write(24,*)i,j,nn,m(i,j,5)
        END DO
      END DO
    END DO

    close(10)
    close(11)
    close(12)
    close(13)
    close(14)
    close(15)
    close(16)
    close(17)
    close(18)
    close(19)
    close(20)
    close(21)
    close(22)
    close(23)
    close(24)
    close(25)
    close(26)

    end
```

9.2 THE FUNCTIONS

func

```
real*8 function func(E)
      implicit real*8 (a-h,o-z)
      common /MandZ/at1,zt1,ap1,zp1,r1,at2,zt2,ap2,zp2,Temp,amu
C     common /resonance/ER,sigmar,C2Sa,C2Sn,gammar,TaR,TnR,ERa,La,Ln
      common /energy/Er(10),EaR(10),EnR(10),Gammar(10),TnR(10),TaR(10)
      common /width/C2Sn(10),C2Sa(10),Gamman(10),Gammaa(10),sigmar(10)
      common /crosssection/ csec(10)
      common /integer/n
```

```
      common /angmon/Ln(10),L(10),La(10)
      common /flag/k,k2
      common /interference/ m(10,10,10),sigmatotplus,sigmatotminus
      common /identifier/ number(10)
      common /something/ d(10)
      real gammae(10)

      E2=E
      En=E+7.4104-6.8120
      bk=8.6171D-5
      bkMeV=8.6171D-11
      func=0.0
      sigmatot=0.0
      sigmatotplus=0.0
      sigmatotminus=0.0
      sigmatotplus2=0.0
      sigmatotminus2=0.0
      AvNo=6.02217D19
      sol=2.998D+8
      eamu=931.502
      pi=3.141592654

      DO i=1,n
        csec(i)=0.0
        d(i)=0.0
      END DO

      DO i=1,n
        call pene(E,La(i),at1,zt1,ap1,zp1,T)
        Ta=T
        call pene(En,Ln(i),at2,zt2,ap2,zp2,T)
        Tn=T
        a=(Ta*Tn)/(TaR(i)*TnR(i))
        b=((gammar(i)/2.0)**2.0)
        c=((E2-EaR(i))*10D06)**2.0+((c2Sa(i)*Ta+c2Sn(i)*Tn)/2.0)**2.0
        d(i)=(EaR(i)/E2)*a*(b/c)
        csec(i)=sigmar(i)*d(i)
        gammae(i)=c2sa(i)*Ta+c2sn(i)*Tn
        sigmatot=sigmatot+csec(i)
        write(15,900)E2,En,ER(i),(EaR(i)/E2),a,(b/c),Ta,Tn
        a=0.0
        b=0.0
        c=0.0
        E=E2
        En=E2+7.4104-6.8120
      END DO

C     IF(k.EQ.0.0) GOTO 287

      sigmatotplus=sigmatot
      sigmatotminus=sigmatot
```

```
      DO i=1,10
        DO j=1,10
          DO nn=0,9
            IF(m(i,j,nn).EQ.1.AND.L(i).EQ.nn.AND.L(j).EQ.nn) THEN
              IF(DABS(E2-EaR(i)).LT.1.0D-4) THEN
                q2=90.0
              ELSE
                q=(gammar(i)/2.0)/((E2-Ear(i))*10.0**6.0)
                q2=-DATAN(q)/pi*180.0
                IF(E2.GT.EaR(i)) q2=q2+180
            END IF
            IF(DABS(E2-EaR(j)).LT.1.0D-4) THEN
                s2=90.0
              ELSE
                s=(gammar(j)/2.0)/((E2-Ear(j))*10.0**6.0)
                s2=-DATAN(s)/pi*180.0
                IF(E2.GT.EaR(j)) s2=s2+180.0
            END IF
            IF(k.EQ.0.AND.nn.EQ.4) write(19,900)E2,q2,s2
            delta=q2-s2
            delta=-DCOS(delta*pi/180.0)
            IF(k.EQ.0.AND.nn.EQ.2) write(17,*)E2,delta
            IF(k.EQ.0.AND.nn.EQ.4) write(18,*)E2,delta
            sigma_int=2.0*DSQRT(csec(i)*csec(j))*delta
          ELSE
            sigma_int=0.0
          END IF
          sigmatotplus=sigmatotplus+sigma_int
          sigmatotminus=sigmatotminus-sigma_int
          END DO
        END DO
      END DO

      IF(k.EQ.0) THEN
        func=sigmatot
        write(13,900)E2,csec,sigmatot
        write(16,900)E2,sigmatot,sigmatotplus,sigmatotminus
C     & sigmatotplus4,sigmatotminus4,sigmatotplus2,
C     & sigmatotminus2,sigmatotplus3,sigmatotminus3
900   format(10D15.6)
      END IF

      IF(k.EQ.1) THEN
        f=DEXP((-E2*10**6.0)/(bk*Temp))
        g=(1.0/((bkMeV*Temp)**(1.5)))
        h=(8.0*(sol*100.0)**2.0/(pi*amu*eamu))**0.5
        func=sigmatot*E2*f*g*h*AvNo
      END IF

C     write(10,*)E2,func
```

```
C     write(6,*)Ta,Tn,a,b,c

      end
```

func2

```
real*8 function func2(E)
      implicit real*8 (a-h,o-z)
      common /MandZ/at1,zt1,ap1,zp1,r1,at2,zt2,ap2,zp2,Temp,amu
C     common /resonance/ER,sigmar,C2Sa,C2Sn,gammar,TaR,TnR,ERa,La,Ln
      common /energy/Er(10),EaR(10),EnR(10),Gammar(10),TnR(10),TaR(10)
      common /width/C2Sn(10),C2Sa(10),Gamman(10),Gammaa(10),sigmar(10)
      common /crosssection/ csec(10)
      common /integer/n
      common /angmon/Ln(10),L(10),La(10)
      common /flag/k,k2
      common /interference/ m(10,10,10),sigmatotplus,sigmatotminus
      common /identifier/ number(10)
      common /something/ d(10)
      external func

      E2=E
      En=E+7.4104-6.8120
      bk=8.6171D-5
      bkMeV=8.6171D-11
      AvNo=6.02217D19
      sol=2.998D+8
      eamu=931.502
      pi=3.141592654

      xarg=func(E2)

      f=DEXP((-E*10**6.0)/(bk*Temp))
      g=(1.0/((bkMeV*Temp)**(1.5)))
      h=(8.0*(sol*100.0)**2.0/(pi*amu*eamu))**0.5
      func2=sigmatotplus*E*f*g*h*AvNo

      end
```

func 3

```
real*8 function func3(E)
      implicit real*8 (a-h,o-z)
      common /MandZ/at1,zt1,ap1,zp1,r1,at2,zt2,ap2,zp2,Temp,amu
C     common /resonance/ER,sigmar,C2Sa,C2Sn,gammar,TaR,TnR,ERa,La,Ln
      common /energy/Er(10),EaR(10),EnR(10),Gammar(10),TnR(10),TaR(10)
      common /width/C2Sn(10),C2Sa(10),Gamman(10),Gammaa(10),sigmar(10)
      common /crosssection/ csec(10)
      common /integer/n
      common /angmon/Ln(10),L(10),La(10)
      common /flag/k,k2
      common /interference/ m(10,10,10),sigmatotplus,sigmatotminus
```

```
common /identifier/ number(10)
common /something/ d(10)
external func

E2=E
En=E+7.4104-6.8120
bk=8.6171D-5
bkMeV=8.6171D-11
AvNo=6.02217D19
sol=2.998D+8
eamu=931.502
pi=3.141592654

xarg=func(E2)

f=DEXP((-E*10**6.0)/(bk*Temp))
g=(1.0/((bkMeV*Temp)**(1.5)))
h=(8.0*(sol*100.0)**2.0/(pi*amu*eamu))**0.5
func3=sigmatotminus*E*f*g*h*AvNo

end
```

10 APPENDIX III: FUNCTIONAL FITS

10.1 ^{6}He(α,n)^{9}Be REACTION RATE FIT

The reaction rate was divided into two regions, one for $T_9 \geq 1$, and one for $T_9 < 1$. The following function was fitted to each region,

$$f = \exp\left(a_1 + a_2 T_9^{-1} + a_3 T_9^{\frac{-1}{3}} + a_4 T_9^{\frac{1}{3}} + a_5 T_9 + a_6 T_9^{\frac{5}{3}} + a_0 \times 2.30285093 \log(T_9)\right). \tag{70}$$

The coefficients a_0 through a_6 are constants and are tabulated for each energy region in Table (8).

T_9	a_0	a_1	a_2	a_3	a_4	a_5	a_6
≥ 1	-305.959	-43.9195	1.6697	-466.654	528.328	-20.4128	0.776993
< 1	186.298	371.844	-3.70735	157.857	-597.867	83.3726	-11.3821

Table 8: Fit coefficients for the reaction rate of ^{6}He(α,n)^{9}Be.

10.2 n-n SCATTERING CROSS-SECTION FIT

To find an adequate fit for the n-n scattering cross-section, the curve was split up into 4 different energy regions, and a fit was found for each region. Table (9) contains the 4 equations used in the programs TWOSTEP2 and TWOSTEPDC to describe the n-n cross-section. The χ^2 coefficients and correlation coefficients are also tabulated, to indicate how well the four functional fits described the experimental data.

E / MeV	$0 \leq E \leq 0.5$	$0.5 < E \leq 1.0$	$1.0 < E \leq 2.0$	$E > 2.0$
functional form	f=$d_0 \exp(d_1 E^{d_2}) \times \exp(d_3 E^{d_4})$	f=$d_0 E^{d_1}$	f= d_0 / E	f= d_0 / E
d_0	19278.7	1951.8	1960.99	1939.4
d_1	104.868	-0.882419		
d_2	1.07744			
d_3	-106.761			
d_4	1.05569			
χ^2	37683.1	1292.1	2292.39	6253.73
Correlation Coefficient	0.999949	0.999872	0.999905	0.99985

Table 9: Function fits and coefficients used to describe the n-n scattering cross-section. The χ^2 value and the correlation coefficient are also tabulated for each fit.

Coefficients	
g_0	5.136
g_1	-9.05657 $\times$ 10^{-5}
g_2	0.159758
g_3	-3.06484
g_4	0.0225038
g_5	-0.0119313
g_6	0.969653

Table 10: The coefficients of the functional fit of the ^{2}n direct capture cross-section.

10.3 DINEUTRON DIRECT CAPTURE CROSS-SECTION FIT

An equation of the form

$$f = \exp\left(g_0 + g_1 E^{-1} + g_2 E^{\frac{-1}{3}} + g_3 E^{\frac{1}{3}} + g_4 E + g_5 E^{\frac{5}{3}}\right) \times E^{g_6}, \qquad (71)$$

where the coefficients g_0 to g_6 are tabulated in Table (10) and E is the Energy in MeV, was fitted to the ^{2}n direct capture cross-section.

However, if $E < 1 \times 10^{-5}$ then

$$f = 21.838 \times E^{0.50008}. \qquad (72)$$

10.4 ^{4}He(2n,γ)^{6}He REACTION RATE FIT

The following equation was fitted to the ^{4}He(2n,γ)^{6}He reaction rate,

$$f = \exp\left(b_1 + b_2 T_9^{-1} + b_3 T_9^{\frac{-1}{3}} + b_4 T_9^{\frac{1}{3}} + b_5 T_9 + b_6 T_9^{\frac{5}{3}}\right) \times T_9^{b_7}. \qquad (73)$$

The coefficients b_1 through b_7 are tabulated in Table (11).

An r-process simulation was also run using the reaction rate calculated previously in [3]. Therefore a fit also had to be found for this rate. For $T_9 \leq 5$

$$f = \exp\left(c_0 + c_1 T_9 + c_2 T_9^2 + c_3 T_9^3 + c_4 T_9^4 + c_5 T_9^5 + c_6 T_9^{c6} + c_7 T_9^7\right), \qquad (74)$$

and for $T_9 > 5$

b_1	b_2	b_3	b_4	b_5	b_6	b_7
-13.4297	0.0220173	-0.750282	-2.92964	0.059314	-0.00259048	1.52535

Table 11: Fit coefficients for the reaction rate of ^{4}He(2n,γ)^{6}He.

$$f = 6.7 \times 10^{-10}\, \mathrm{T_9} > 5. \tag{75}$$

The coefficients c_0 through c_7 are tabulated in Table (12).

coefficient	
c_0	-25.6195
c_1	3.22718
c_2	-2.03827
c_3	0.531853
c_4	-0.075149
c_5	0.00419848
c_6	1.0834
c_7	5.8321×10^{-6}

Table 12: Fit coefficients for the reaction rate of ^{4}He(2n,γ)^{6}He calculated in [3].

Bibliography

[1] C. E. Rolfs and W. S. Rodney, *Cauldrons in the Cosmos* (University of Chicago Press, Chicago, 1988)

[2] S. Woosley and R. Hoffman, ApJ **395** 202 (1992)

[3] J. Görres, H. Herndl, I. J. Thompson and M. Wiescher, Phys. Rev. **C52** 2231 (1995)

[4] R. Kinsey, C. Dunford, J. Tuli, and T. Burrows, Capture Gamma-Ray Spectroscopy and Related Topics, **2** 657 (1997)

[5] K. Krane, *Introductory Nuclear Physics* (John Wiley & Sons, 1988)

[6] V. Efros, W. Balogh, H. Herndl, R. Hofinger, H. Oberhummer, Z. Phys. **A355** 101 (1996)

[7] M. Terasawa, K. Sumiyoshi,T. Kajino, G. J. Mathews and I. Tanihata, ApJ **562** 470 (2001)

[8] F. Ajzenberg-Selove, Nucl. Phys. **A490**, 1 (1988)

[9] N. Soić, S. Blagus, M. Bogovac, S. Fazinić, M. Lattuada, M. Milin, D. Miljanić, D. Rendic, C. Spitaleri, T. Tadić and M. Zadro, Europhys. Lett. **34**, 7 (1996)

[10] J.M. Alexander, A. Elmaani, L. Kowalalski, N.N. Ajitanand and C.J. Gelderloos, Phys. Rev. **C48**, 2874 (1993)

[11] N. Curtis, D.D. Caussyn, N.R. Fletcher, N. Fay, J.A. Liendo, F. Marechal, D. Robson, and D. Shorb, Nucl. Phys. **A682**, 339 (2001)

[12] M. Freer, J.C. Angélique, L. Axelsson, B. Benoit, U. Bergmann, W.N. Catford, S.P.G. Chappell, N.M. Clarke, N. Curtis, A. D'Arrigo, E. de Góes Brennard, O. Dorvaux, B.R. Fulton, G. Giardina, C. Gregori, S. Grévy, F. Hanappe, G. Kelly, M. Labiche, C. Le Brun, S. Leenhardt, M. Lewitowicz, K. Markenroth, F.M. Marqués, J.T. Murgatroyd, T. Nilsson, A. Ninane, N.A. Orr, I. Piqueras, M.G. Saint Laurent, S.M. Singer, O. Sorlin, L. Stutté and D.L. Watson, Phys. Rev. **C63** 034301 (2001)

[13] N. Curtis, D.D. Caussyn, N.R. Fletcher, F. Maréchal, N. Fay and D. Robson, Phys. Rev. **C64**, 044604 (2001)

[14] S. Hamada, M. Yasue, S. Kubono, M.H. Tanaka and R.J. Peterson, Phys. Rev. **C49**, 3129 (1994)

[15] T. Aumann, D. Aleksandrov, L. Axelsson, T. Baumann, M. J. G. Borge, L.V. Chulkov, J. Cub, W. Dostal, B. Eberlein, Th. W. Elze, H. Emling, H. Geissel, V. Z. Goldberg, M. Golovkov, A. Grünschloβ, M. Hellström, K. Hencken, J. Holeczek, R. Holzmann, B. Jonson, A. A. Korshenninikov, J. V. Kratz, G. Kraus, R. Kulessa, Y. Leifuls, A. Leistenschneider, T. Leth, I. Mukha, G. Münzenberg, F. Nickel, T. Nilsson, G. Nyman, B. Petersen, M. Steiner, J. Stroth, A. Surowiec, T. Suzuki, O. Tengblad and M. V. Zhukov, Phys. Rev. **C59** 1252 (1999)

[16] J. M. Alexander, A. Elmaani, L. Kowalski, N. N. Ajitanand and C. J. Gelderloos, Phys. Rev. **C48** 2874 (1993)

[17] S. Wanajo, T. Kajino, G. Mathews and K. Otsuki, ApJ **554** 578 (2001)

[18] T. Kajino, S. Wanajo and G. Mathews, Nucl. Phys. **A704** 165c (2002)

[19] W. A. Fowler, G. R Caughlan, B. A. Zimmerman, Ann. Rev. Astron. Ap. **13**, 69 (1975)

[20] D. R. Tilley, J. H. Kelley, J. L. Godwin, D. J. Millener, J. Purcell, C. G. Sheu, H. R. Weller *Energy Levels of Light Nuclei A=10* (not yet published)

[21] F. Käppeler, H. Beer, K. Wisshak, Rep. Prog. Phys. **52** 945 (1989)

[22] K. Otsuki (Private Communication)

[23] C. E. Rolfs, Nucl. Phys. **A217** 29 (1973)

[24] R. F. Christy, I. Duck, Nucl. Phys. **24** 89 (1961)

[25] A. Mengoni, T. Otsuka, M. Ishihara, Phys. Rev. **C52** R2334 (1995)

[26] C. Baeumer, A. M. van den Berg, B. Davids, D. Frekers, D. De Frenne, E.-W. Grewe, P. Haefner, M. N. Harakeh, F. Hofmann, M. Hunyadi, E. Jacobs, B. C. Junk, A. Korff, K. Langanke, G. Martnez-Pinedo, A. Negret, P. von Neumann-Cosel, L. Popescu, S. Rakers, A. Richter, and H. J. Woertche, Phys. Rev. **C68** R031303 (2003)

[27] K. Sumiyoshi, K. Suzuki, K. Otsuki, M. Terasawa, S. Yamada, PASJ **52** 601 (2000)